

Applications of the PAM Representation of CPM

Balachandra Kumaraswamy

Submitted to the Department of Electrical Engineering &
Computer Science and the Faculty of the Graduate School
of the University of Kansas in partial fulfillment of
the requirements for the degree of Master's of Science

Thesis Committee:

Dr. Erik Perrins: Chairperson

Dr. Alexander Wyglinski

Dr. James Roberts

Date Defended

© 2008 Balachandra Kumaraswamy

The Thesis Committee for Balachandra Kumaraswamy certifies
That this is the approved version of the following thesis:

Applications of the PAM Representation of CPM

Committee:

Chairperson

Date Approved

To my Parents.

Acknowledgements

All praise is due to Lord Hanuman and Guru Raghavendra.

I thank my parents for giving me the opportunity to study at the University of Kansas. I would love to thank my Uncle (Chikkappa) who has always encouraged me to achieve great heights in my life.

I would like to thank my advisor Dr. Erik Perrins for giving me a wonderful opportunity to work with him. It was a pleasure working with you. As a friend you have always helped me to overcome tough times in my academic career. You will always be my role model and a great source of inspiration for my career ahead. Thank you for having faith in my potential and supporting me complete my thesis. I would like to thank Dr. Alexander Wyglinski and Dr. James Roberts for being on my committee. I would like to thank the ITTC staff in making it a center of excellence.

I thank all my professors at KU for making my stay here memorable. And last but not the least my friends at KU who have always been with me through my good and bad times. They have become an inseparable part of my life. Thanks friends for supporting me.

Symbols

α transmitted symbol

$s(t; \boldsymbol{\alpha})$ modulated signal

$r(t)$ received signal

L length of frequency pulse

$f(t)$ frequency pulse

$q(t)$ phase pulse

h modulation index

θ_{n-L} phase state

n time step

$a[n]$ original data bits

$b_k[n], v[n], \beta(\alpha_n)$ pseudo symbols

$p(t)$ main PAM pulse

T duration of each symbol

\tilde{S}_n hypothetical starting state

\tilde{E}_n hypothetical ending state

$\lambda_n(\tilde{S}_n)$ cumulative metric

$\lambda_{n+1}(\tilde{E}_n)$ branch metric

$g_k(t)$ principal pulses for PAM representation

$z(n, [\tilde{a}_n, \tilde{S}_n])$ branch metric update

$c_k(t)$ signal pulses

$\phi(t; \alpha)$ phase

Note: the default range in the summations is from $-\infty$ to $+\infty$

Abstract

In this thesis, we are trying to optimize the tradeoff between the receiver complexity and its performance for two modulations currently used in aeronautical telemetry. A reduced complexity detector is of interest because it reduces the implementation cost. The Pulse Amplitude Modulation (PAM) representation of Continuous Phase Modulation (CPM) signals typically results in reduced-complexity detectors with a performance that matches the performance of the optimal detector. In this work, we study simple trellis-based PAM detectors for two types of CPM used in aeronautical telemetry. The first is shaped-offset quadrature phase shift keying (SOQPSK), where we show that the state complexity can be cut in half relative to previous approaches—from 4 states down to 2—with asymptotically optimum performance. For comparison, we implement another reduced complexity technique known as Pulse Truncation (PT); both of these techniques make use of recent advances in SOQPSK technology based on a CPM interpretation of SOQPSK. The proposed simplifications are significant since trellis-based SOQPSK detectors are 1–2 dB superior with respect to the widely-deployed symbol-by-symbol detectors. These performance gains come at the expense of complexity, and the proposed 2-state detectors minimize this expense. The second version of CPM studied in this work is Pulse Code Modulation/Frequency Modulation (PCM/FM). We develop and compare the per-

performances of 0, 2 and 4 state PAM based detectors. We develop our PCM/FM receiver using two approaches; first with a square-root cosine (SRC) filter which is independent of the CPM modulation index, and the second using the main PAM pulse followed by a whitening filter. The 4-state trellis based detectors we derive for PCM/FM give a performance within 0.4–0.5 dB of the optimal detector (refer to Appendix I for optimal detector complexity).

Contents

Acceptance Page	i
Acknowledgements	iii
Symbols	iv
Abstract	vi
1 Introduction	1
1.1 Motivation to develop simplified SOQPSK detectors	3
1.2 Motivation to develop simplified PCM/FM detectors	5
1.3 Major contributions of this thesis work	6
2 Signal Representation of CPM	7
2.1 CPM Signal Model	7
2.2 SOQPSK	9
2.2.1 SOQPSK Precoder	10
2.2.2 Trellis Representation of SOQPSK	13
2.3 PCM/FM	15
2.4 Summary	18
3 SOQPSK Detectors	19
3.1 Received Signal Model	19
3.2 Branch Metric Increment Using Pulse Truncation	20
3.3 Branch Metric Increment Using the PAM Representation	22
3.4 2-State Detectors for SOQPSK	25
3.5 Summary	26

4	SOQPSK Performance Analysis	27
4.1	Minimum Distance Error Event	27
4.2	Additional Error Event for 2-State Detectors	28
4.3	Probability of Bit Error	29
4.4	Simulation Results	31
4.5	Summary	34
5	PCM/FM Detection	36
5.1	Receiver Design	36
5.2	Reduced State Sequence Detection (RSSD)	38
5.3	Summary	42
6	PCM/FM Results	43
6.1	Summary	44
7	Conclusion	46
7.1	Acknowledgment	47
	Appendix I - Optimal Detector Complexity	48
	Appendix II - 2-state trellis	49
	Appendix III - Whitening Filter Design	52
	Appendix IV - Example to calculate the squared distance	56
	Appendix V - Laurent's Approximation	58
	References	60

List of Figures

2.1	The length-8T frequency and phase pulses for SOQPSK-TG. . . .	9
2.2	Precoders (a) SOQPSK Precoder corresponding to 4-state trellis and (b) SOQPSK Differential Precoder corresponding to 2-state trellis.	11
2.3	4-state time-varying trellis for the precoder/CPM modulator. . . .	13
2.4	2-state trellis representing the differential precoder.	14
2.5	The length-2T frequency and phase pulses for PCM/FM.	16
2.6	The first two impulses $c_0(t)$ and $c_1(t)$	16
2.7	The main pulse $p(t)$	17
3.1	The two principal pulses for the PAM representation of (a) SOQPSK-MIL and (b) SOQPSK-TG.	24
4.1	Range of distances for 2-state SOQPSK-MIL PAM-based detector.	30
4.2	Range of distances for 2-state SOQPSK-TG PT-based detector.	31
4.3	Range of distances for 2-state SOQPSK-TG PAM-based detector.	32
4.4	Performance of reduced-complexity detectors for SOQPSK-MIL.	34
4.5	Performance of reduced-complexity detectors for SOQPSK-TG.	35
5.1	Magnitude frequency response for WMF $H_{\text{WMF}}(f)$ with $h = 0.7$ and for SRC filter with roll-off factor of 0.2.	37
5.2	Receiver design for PCM/FM using WF.	38
5.3	Receiver design for PCM/FM using $h_{\text{SRC}}(t)$	40
6.1	Performance of reduced-complexity detectors for PCM/FM.	45
7.1	Autocorrelation of main pulse $p(t)$	54
7.2	Autocorrelation of AWGN passed through $p(t)$	54

7.3	Autocorrelation of the sampled autocorrelation after passing through WF.	55
-----	---	----

List of Tables

3.1	The relationship between the ternary branch symbol α_n , and the pseudo-symbols $\beta_k(\alpha_n)$ for SOQPSK.	25
4.1	Range of distance values in the set $\{d_{2,l}^2\}$ for the 2-state SOQPSK detectors.	30

Chapter 1

Introduction

Digital communication deals with transmission of information in digital form from source to destination in a reliable manner. The *digital modulator* takes up the job of converting the binary information into signal waveforms. Here we limit our discussion only to phase modulation. The digitally modulated data reaches the demodulator through a communication channel which introduces noise into the data being transmitted. The corrupted data received at the receiver is processed to get back the original information that was transmitted.

Here we discuss continuous phase modulation (CPM) [2]. Basically, we cover two types of CPM, Shaped-offset QPSK and Pulse Code Modulation/Frequency Modulation (PCM/FM). Both of these are used in the aeronautical telemetry standard IRIG-106 [22].

While CPM has a number of advantages, one advantage in particular is responsible for its widespread deployment: it has a constant signal envelope (the amplitude of the signal constellation remains constant). This makes it compatible with nonlinear power amplifiers, which are highly efficient in converting limited (i.e. battery) power into radiated power (for example, 16-QAM (Quadrature Am-

plitude Modulation) the amplitude varies with each constellation point. The 16-QAM modulated signal gets distorted when passed through a nonlinear amplifier). This in turn allows for a smaller physical size and lower cost for the transmitter. The disadvantage with CPM is high complexity involved with its implementation. This is because of the nonlinear nature of the modulation.

The implementation of the optimal CPM detector often requires a huge trellis as well as large number of matched filters (MFs). In this work, we decompose the CPM signal into linear combination of Pulse Amplitude Modulation (PAM) waveforms [8,12,13,18]. PAM-based detectors are known to reduce the complexity of the receiver [19], by reducing the trellis size as well as the number of MFs.

With increasing receiver complexity comes increasing cost. In this thesis, we come up with PAM-based reduced complexity detectors. PAM-based detectors reduce the receiver implementation cost with little compromise on performance.

Laurent [12] showed that a binary CPM signal can be represented as a superposition of PAM waveforms

$$s(t; \boldsymbol{\alpha}) = \sum_n \sum_{k=0}^{Q-1} b_k[n] c_k(t - nT), \quad Q = 2^{L-1}. \quad (1.1)$$

The *pseudo-symbols* $b_k[n]$ (that are derived from the original data, refer to equation (2.18)) inherit the nonlinearity of CPM. The signal pulses $c_k(t)$ are modulated by pseudo-symbols $b_k[n]$ and are summed up to give the CPM signal. The signal pulses $c_k(t)$ have different energy levels. The signal pulses with higher energy dominate the linear representation of CPM. This property can be used to approximate the CPM signal which helps in reducing the complexity of the receiver by reducing the trellis size and MFs.

Also Perrins and Rice [16] showed that ternary CPM waveforms (of which,

SOQPSK is an example) can be represented using the PAM decomposition by

$$s(t; \boldsymbol{\alpha}) = \sum_n \sum_{k=0}^{R-1} v_k[n] g_k(t - nT), \quad R = 2 \cdot 3^{L-1}. \quad (1.2)$$

The *pseudo-symbols* $v_k[n]$ are obtained from the original data symbols. In this work, PAM decomposition is applied to SOQPSK and PCM/FM to develop simplified detectors.

1.1 Motivation to develop simplified SOQPSK detectors

The signal model and the parameters for SOQPSK will be discussed in more detail in the next chapter. We discuss two types of SOQPSK, the military-standard “SOQPSK-MIL” [1] and the version of SOQPSK adopted by the telemetry group, “SOQPSK-TG” [22].

Due to the similarities between SOQPSK and conventional offset QPSK (OQPSK), OQPSK-type detectors are most commonly deployed at the receiver for detecting SOQPSK. Though OQPSK-type detectors are easy to implement, they suffer a loss of 1–2 dB compared to the optimal detector, depending on which version of SOQPSK is being used and how closely matched the detection filters are to the transmitted signal [5]. This is a significant loss since it erodes some of the power advantages enjoyed by SOQPSK in the first place. Hence in our work we propose reduced complexity PAM detectors which gives a performance that matches the optimal detectors (refer to simulation results).

Recently in [19], a CPM interpretation of SOQPSK was applied at the receiver. This resulted in an optimal detector for SOQPSK-MIL and opened the door for two reduced-complexity methods for detecting the more complicated SOQPSK-

TG. These two techniques, PAM and pulse truncation (PT) [3,25] result in 4-state detectors for SOQPSK-TG that are within 0.2 dB of the impractical *512-state* optimum detector.¹

In this work, we study simple trellis based detectors for SOQPSK that have a minimal level of state complexity. Previous efforts have been made to develop simplified detectors for SOQPSK using the PAM approach, e.g. [19]. The previous works could reduce the state complexity to 4 states. Here, we show the size of the trellis can be reduced to its minimum—2 states—for both SOQPSK-MIL and SOQPSK-TG. This is accomplished by a novel concatenation of the differential encoder and SOQPSK *precoder*, which leads to a simplified representation of the transmitter’s state memory (refer to Appendix II). This simplified transmitter model combined with decision-feedback at the receiver yields the overall state reduction. We show how this state reduction can be implemented using the PAM and PT techniques (refer to Chapter 3). In both cases, the 2-state detectors have no asymptotic losses relative to their 4-state counterparts. However, for moderate signal-to-noise ratios, the PT technique results in a minor loss on the order of 0.1 dB w.r.t. PAM.

This state reduction is significant since the major drawback of trellis-based detectors is their complexity compared to symbol-by-symbol detectors. Since the proposed detectors reduce the state complexity to its minimum of 2 states, these detectors represent an attractive means of realizing the 1–2 dB advantage trellis-based detectors have over symbol-by-symbol detectors.

¹The optimal detector has 512 states and number of matched filters = $2 \cdot M^L = 2 \cdot 2^8 = 512$ (refer to Appendix I). Hence decoding a bit requires multiplications in the order of teraflops when the data rate is large (a teraflop is one trillion floating point operations per second). Using the PAM decomposition, with $L = 8$ we have $R = 2 \cdot 3^{8-1} = 4374$. Therefore the exact PAM representation of SOQPSK-TG has an unmanageable number of signal components.

1.2 Motivation to develop simplified PCM/FM detectors

Having developed simple PAM based detectors for SOQPSK, we developed PAM based reduced complexity detectors for PCM/FM which is also a type of CPM. As it turns out, PCM/FM and Bluetooth share a number of similarities. As such, we will draw upon some previous work on Bluetooth [9].

By design, the CPM modulation index for Bluetooth is allowed to vary in the range 0.28 to 0.35. In the case of PCM/FM the CPM modulation typically varies from 0.63 to 0.77, although in this case it is not by design but it is instead due to outdated analog transmitter circuitry that remains in use on telemetry test ranges. Also, Bluetooth devices often employ a simple discriminator detector, which is also the case with PCM/FM. Another way to implement the detector for PCM/FM and Bluetooth is to use Viterbi Algorithm (VA).

These are some of the similarities which prompted us to combine Bluetooth algorithms and PCM/FM. Ibrahim *et al.* [9] developed reduced-complexity detectors for Bluetooth using the PAM decomposition. This motivated us to implement a Viterbi algorithm (VA) based detector for PCM/FM using the PAM decomposition. Though trellis based detectors increase the complexity, it shows 3–4 dB improvement as compared to discriminator detector.

We propose two approaches to develop simple trellis based detectors for PCM/FM. The first, using the main PAM pulse $p(t)$ followed by a whitening filter. In the second approach we use an off-the-shelf square-root raised cosine (SRC) filter as the receiver filter. In the SRC filter approach we have used a seven-tap feed forward filter (FFF) to obtain a minimum-phase channel response.

1.3 Major contributions of this thesis work

1. Developed a 2-state PAM based detector for SOQPSK-MIL and SOQPSK-TG.
2. Developed 2-state detectors using PT for comparison with PAM based detectors.
3. Demonstrated that 2-state PAM and PT based detectors gives a performance that matches 4-state detectors (developed using previous approaches).
4. Developed reduced complexity PAM based detectors for PCM/FM using 0, 2 and 4 states and compare their performances. 4-state detectors give a near optimal performance (optimal detector uses 20 states).
5. Achieved the goal to develop reduced complexity detectors for two types of CPM viz. SOQPSK and PCM/FM, with a near optimal performance. Lesser the complexity of the receiver lesser is the cost.

Chapter 2

Signal Representation of CPM

In this chapter we explain the general CPM signal model, and then give SO-QPSK and PCM/FM specific details.

2.1 CPM Signal Model

The CPM signal may be represented as [2]

$$s(t; \boldsymbol{\alpha}) \triangleq \exp \{j\phi(t; \boldsymbol{\alpha})\} \quad (2.1)$$

where the phase is a pulse train of the form

$$\phi(t; \boldsymbol{\alpha}) \triangleq 2\pi h \sum_i \alpha_i q(t - iT) \quad (2.2)$$

and α_i is an M -ary symbol, T is the duration of each α_i , and h is the modulation index (the modulation index indicates by how much the phase of the modulated signal varies around its unmodulated signal). The *phase pulse* $q(t)$ is

defined as [2]

$$q(t) \triangleq \begin{cases} 0 & t < 0 \\ \int_0^t f(\tau) d\tau & 0 \leq t < LT \\ 1/2 & t \geq LT \end{cases} \quad (2.3)$$

where $f(t)$ is the *frequency pulse* which has a duration of L symbol times and an area of $1/2$. When $L = 1$ the signal is *full-response* and when $L > 1$ it is *partial-response*. Due to the constraints on $f(t)$ and $q(t)$, and assuming a rational modulation index $h = k/p$, the phase may be expressed as

$$\phi(t; \boldsymbol{\alpha}) = 2\pi h \underbrace{\sum_{i=n-L+1}^n \alpha_i q(t - iT)}_{\theta(t)} + \pi h \underbrace{\sum_{i=0}^{n-L} \alpha_i}_{\theta_{n-L}} \quad (2.4)$$

where $nT \leq t < (n+1)T$. The *phase state* θ_{n-L} can assume only p distinct values given by

$$\frac{2\pi x}{p}, \quad 0 \leq x \leq p-1. \quad (2.5)$$

The state of a CPM signal is specified by

$$\sigma = [\theta_{n-L}, \alpha_{n-L+1}, \dots, \alpha_{n-1}]. \quad (2.6)$$

From equation (7.1), we see that the number of states in the trellis is $p \cdot M^{L-1}$, because there are p cumulative phase states and M^{L-1} symbol combinations resulting from the $(L-1)$ -tuple. Since each state is associated with M possible branch symbols, the number of branches is $p \cdot M^L$. The number of matched filters is given by $2M^L$.

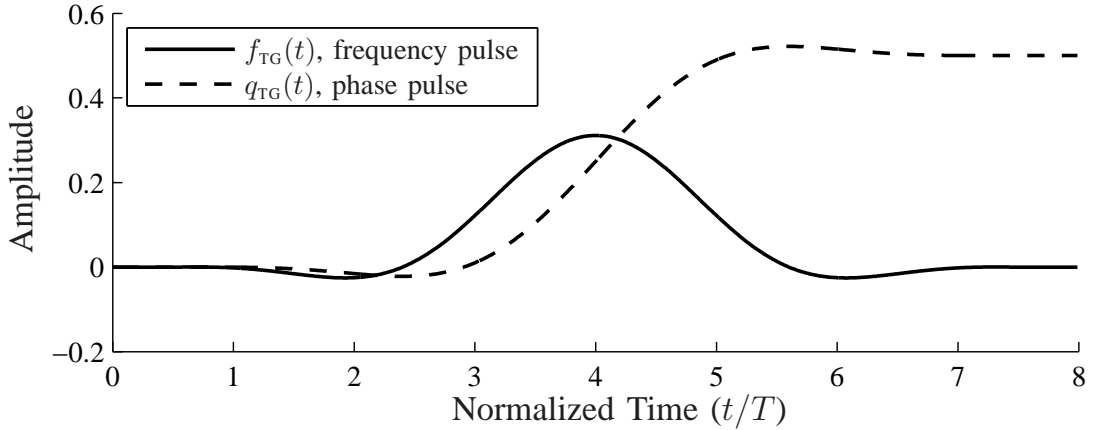


Figure 2.1. The length-8T frequency and phase pulses for SOQPSK-TG.

2.2 SOQPSK

SOQPSK is a special type of CPM where the symbol sequence is $\alpha_i \in \{-1, 0, +1\}$ and when $\alpha_i = \pm 1$, the phase of the signal changes by $\pm 90^\circ$. In the world of CPM, the modulation index h is the parameter that specifies the amount of phase change devoted to each α_i and a change of 90° corresponds to $h = 1/2$. Here we discuss two versions of SOQPSK. The first, SOQPSK-MIL [1], is full-response with a rectangular shaped frequency pulse

$$f_{\text{MIL}}(t) \triangleq \begin{cases} \frac{1}{2T}, & 0 \leq t < T \\ 0, & \text{otherwise.} \end{cases} \quad (2.7)$$

The second, SOQPSK-TG [7, 22], is partial-response with $L = 8$ and a frequency pulse given by

$$f_{\text{TG}}(t) \triangleq A \frac{\cos(\frac{\pi \rho B t}{2T})}{1 - 4(\frac{\rho B t}{2T})^2} \times \frac{\sin(\frac{\pi B t}{2T})}{\frac{\pi B t}{2T}} \times w(t) \quad (2.8)$$

where the window is

$$w(t) \triangleq \begin{cases} 1, & 0 \leq |\frac{t}{2T}| < T_1 \\ \frac{1}{2} + \frac{1}{2} \cos(\frac{\pi}{T_2}(\frac{t}{2T} - T_1)), & T_1 \leq |\frac{t}{2T}| \leq T_1 + T_2 \\ 0, & T_1 + T_2 < |\frac{t}{2T}|. \end{cases}$$

The constant A is chosen such that the area of the pulse is equal to $1/2$ and $T_1 = 1.5$, $T_2 = 0.5$, $\rho = 0.7$ and $B = 1.25$. Figure 2.1 shows the frequency pulse $f_{\text{TG}}(t)$ and corresponding phase pulse $q_{\text{TG}}(t)$.

2.2.1 SOQPSK Precoder

With SOQPSK, the channel symbols $\boldsymbol{\alpha} = \{\alpha_n\}$ are not the underlying information sequence, but are related to the original data sequence $\boldsymbol{a} = \{a_n\}$ by the series of operations shown in Figure 2.2(a). The first of these operations is a double differential encoder [24] given by the equation

$$u_i = a_i \oplus u_{i-2}, \quad a_i, u_i \in \{0, 1\} \quad (2.9)$$

where \oplus is the modulo-2 addition operator. The differential encoding rule in (2.9) can be summarized as “change phase on 1” since an input of $a_i = 1$ causes the output value u_i to change relative to the value u_{i-2} .

The second operation in Figure 2.2(a) is the precoder, which converts the double differentially encoded $\{u_i\}$ into ternary data $\alpha_i \in \{-1, 0, +1\}$ according to the rule [23]

$$\alpha_i(u) = (-1)^{i+1}(2u_{i-1} - 1)(u_i - u_{i-2}) \quad (2.10)$$

The precoder imposes three important constraints on the ternary data [23]:

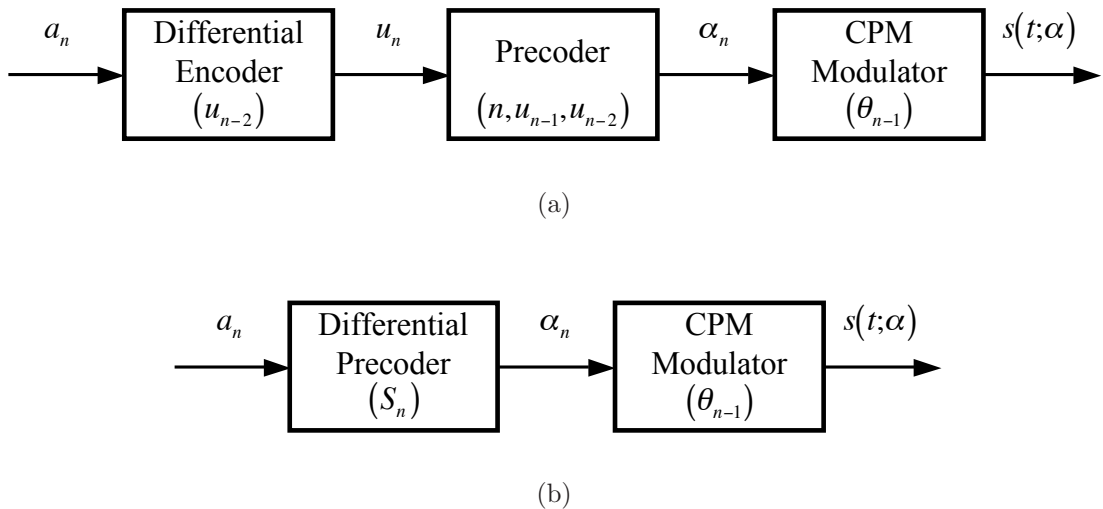


Figure 2.2. Precoders (a) SOQPSK Precoder corresponding to 4-state trellis and (b) SOQPSK Differential Precoder corresponding to 2-state trellis.

1. While α_i is viewed as being *ternary*, in any given symbol interval α_i is actually drawn from one of two *binary* alphabets, $\{0, +1\}$ or $\{0, -1\}$.
2. When $\alpha_i = 0$, the binary alphabet for α_{i+1} switches from the one used for α_i , when $\alpha_i \neq 0$ the binary alphabet for α_{i+1} does not change.
3. A value of $\alpha_i = +1$ cannot be followed by $\alpha_{i+1} = -1$, and vice versa (this is implied by the previous constraint).

From Figure 2.2(a) and (2.10) we see that the operation of the precoder requires knowledge of whether the current symbol time is even or odd (n -even/ n -odd), and also knowledge of the two previous precoder inputs u_{n-1} and u_{n-2} . These three binary-valued elements form the *state memory* of the precoder (n, u_{n-1}, u_{n-2}) . This state memory leads to the trellis representation discussed in the following section.

Figure 2.2(b) shows an alternate precoder representation where the double

differential encoder and the precoder are combined to form a *differential precoder*.

It was shown in [15] that the differential precoder has the form

$$\alpha_n = (-1)^{\mathcal{S}_n} a_n \quad (2.11)$$

where the *sign state* is

$$\mathcal{S}_{n+1} = (\mathcal{S}_n + \alpha_n + 1) \bmod 2. \quad (2.12)$$

We point out that the binary-valued sign state \mathcal{S}_n is the only state variable required by the differential precoder.

All of the binary-to-ternary constraints are visible in (2.11) and (2.12) and are explained in the next few sentences. Since the current bit a_n is drawn from a binary alphabet, α_n is also drawn from a binary alphabet whose “sign” is controlled by the sign state \mathcal{S}_n ; the switching rule for the binary alphabets is “switch alphabets on $\alpha_n = 0$,” which is exactly how (2.12) works. Furthermore, an elegant side effect of the differential precoder is that the original information bits are identified in the ternary symbol sequence: $a_n = 0$ always maps to $\alpha_n = 0$ and $a_n = 1$ always maps to $\alpha_n = \pm 1$. Therefore, the “change phase on 1” rule is visible in the differential precoder since $\alpha_n = \pm 1$ changes the phase of the CPM signal.

In either precoder representation, Figure 2.2(a) or Figure 2.2(b), the output of the precoder is connected to an ordinary CPM modulator with $h = 1/2$ and the desired pulse shape $f_{\text{ML}}(t)$ or $f_{\text{TG}}(t)$. For the special case of full-response CPM ($L = 1$), the only memory within the CPM modulator is the phase state θ_{n-1} . The interaction between the memory of the precoder(s) and the memory of the CPM modulator is discussed next.

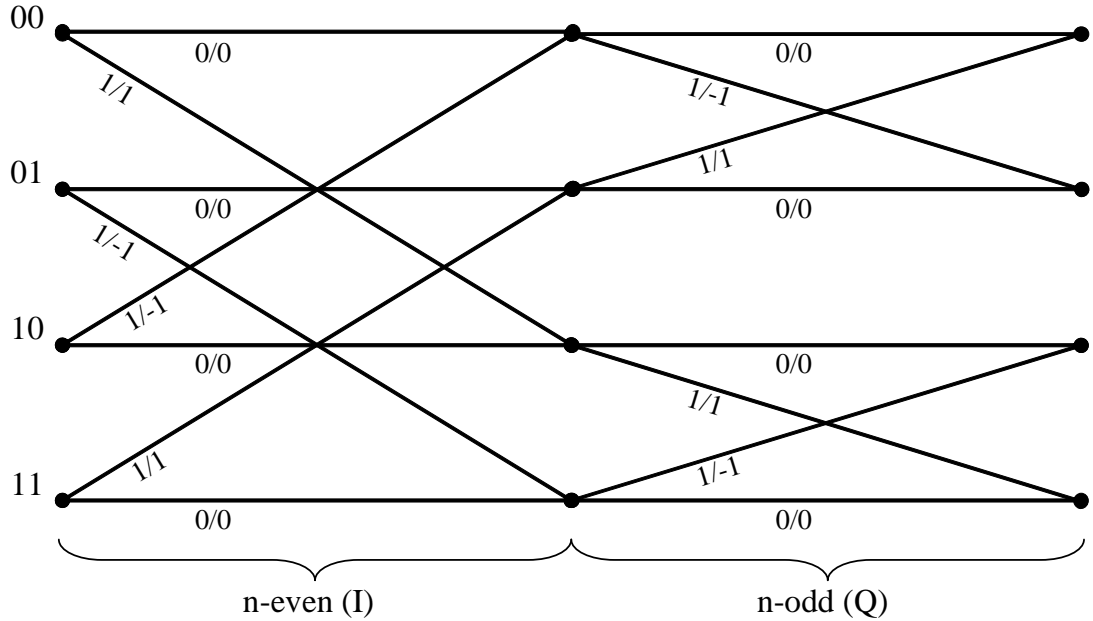


Figure 2.3. 4-state time-varying trellis for the precoder/CPM modulator.

2.2.2 Trellis Representation of SOQPSK

Figure 2.3 shows the 4-state time-varying trellis that describes the SOQPSK precoder in Figure 2.2(a) [19]. In this trellis, n -even/ n -odd is not treated as a state variable (since it would result in an 8-state trellis) but is instead handled with the time-varying nature of the trellis. The remaining state variables are u_{n-1} and u_{n-2} . These are ordered (u_{n-2}, u_{n-1}) for n -even and (u_{n-1}, u_{n-2}) for n -odd [23]. This means that the inphase (I) bit of the pair is always most significant and the quadrature (Q) bit of the pair is always least significant. The labels along each branch of the trellis show the input bit/output symbol pair, a_n/α_n , for the given branch.

The advantage of the 4-state trellis is that its state variables u_{n-1} and u_{n-2} have a *one-to-one correspondence* with the phase state θ_{n-1} of the full-response CPM modulator that follows the precoder. In other words, a separate trellis is

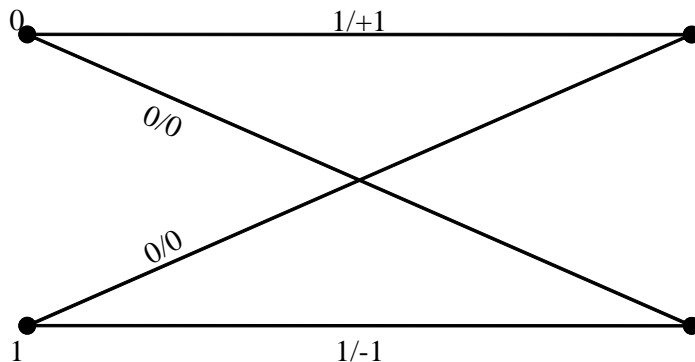


Figure 2.4. 2-state trellis representing the differential precoder.

not required by the CPM modulator, and the entire system in Figure 2.2(a) is described by the 4-state time-varying trellis in Figure 2.3. The mapping from precoder trellis states to CPM phase states is [19]

$$\begin{aligned}
 00 &\leftrightarrow \frac{3\pi}{2}, & 01 &\leftrightarrow \pi, \\
 10 &\leftrightarrow 0, & 11 &\leftrightarrow \frac{\pi}{2}.
 \end{aligned}
 \tag{2.13}$$

Figure 2.4 shows the 2-state *time-invariant* trellis that describes the differential SOQPSK precoder in Figure 2.2(b) and equations (2.11) and (2.12). The state variable is simply the sign state \mathcal{S}_n , and the labels along each branch specify the input bit/output symbol pair a_n/α_n for the given branch.

The advantage of the 2-state trellis is its simplicity with respect to the 4-state time-varying trellis in Figure 2.3 (by reducing the trellis state complexity to minimal, half compared to the previous approaches). Unfortunately, this simplification does not also manifest itself with the CPM phase state θ_{n-1} . Thus, a 4-state trellis is still required to fully (i.e. optimally) describe the entire system

in Figure 2.2(b). The next section shows how a *decision feedback* scheme can be employed at the detector to find the CPM phase state θ_{n-1} ; this technique allows the simple 2-state trellis to be successfully applied to SOQPSK and yields near-optimal performance.

2.3 PCM/FM

PCM/FM is a form of CPM where the symbol sequence $\alpha_i \in \{\pm 1\}$ with modulation index $h = 7/10$, $M = 2$ and a 2RC frequency pulse (raised cosine pulse with duration $L = 2$). The frequency pulse $f(t)$ is given by [2]

$$f_{\text{PCM/FM}}(t) \triangleq \begin{cases} \frac{1}{2LT} \left[1 - \cos\left(\frac{2\pi t}{LT}\right) \right], & 0 \leq t < LT \\ 0, & \text{otherwise.} \end{cases} \quad (2.14)$$

where $L = 2$.

As discussed earlier, Laurent developed an alternative linear representation of the CPM signal given by

$$s(t; \boldsymbol{\alpha}) = \sum_n \sum_{k=0}^{Q-1} b_k[n] c_k(t - nT) \quad Q = 2^{L-1}. \quad (2.15)$$

For PCM/FM with $L = 2$, the above equation becomes

$$s(t; \boldsymbol{\alpha}) = \sum_n \sum_{k=0}^1 b_k[n] c_k(t - nT) \quad (2.16)$$

since $Q = 2$. This prompted us to develop simple PAM-based detectors for PCM/FM after successfully developing simplified PAM-based detectors for SOQPSK. Laurent [12] showed that for CPM signals the sum is dominated by the

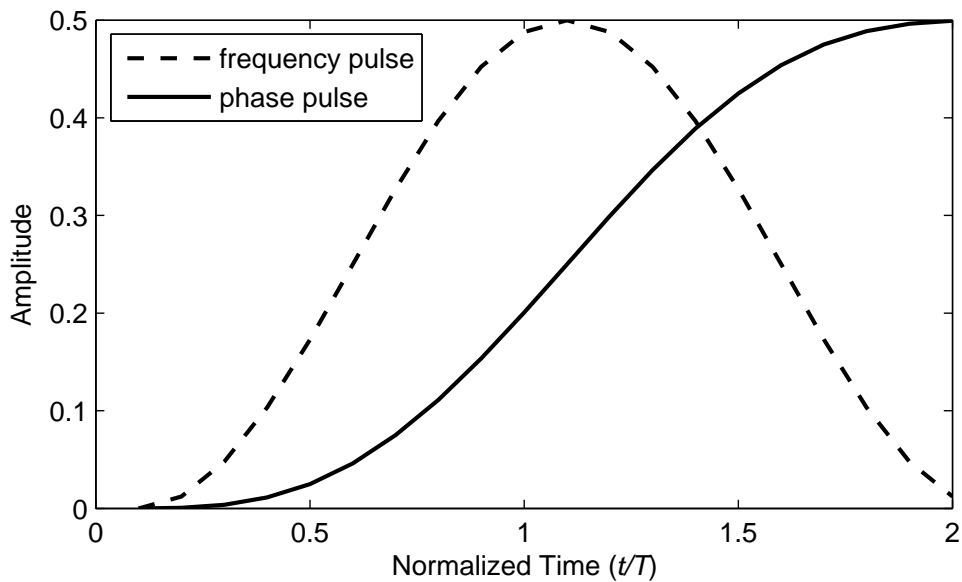


Figure 2.5. The length- $2T$ frequency and phase pulses for PCM/FM.

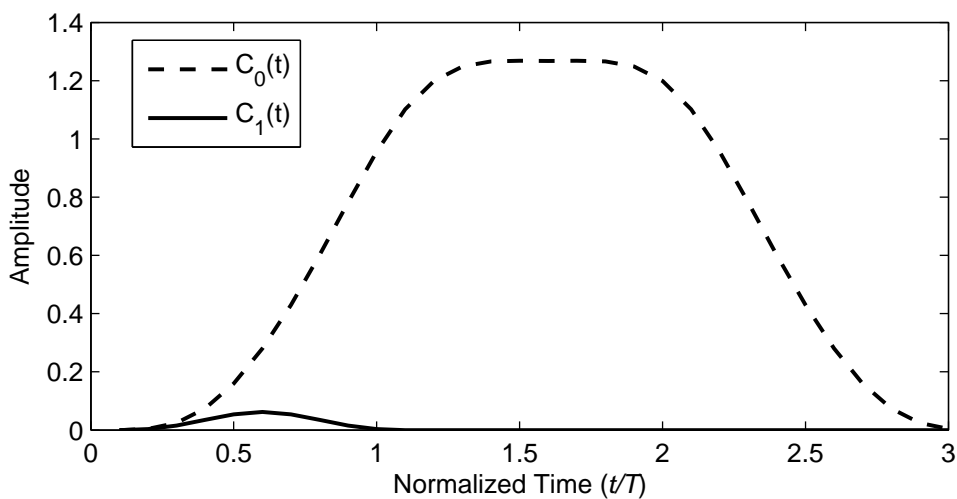


Figure 2.6. The first two impulses $c_0(t)$ and $c_1(t)$.

first pulse $c_0(t)$. This can be confirmed from the Figure 2.6. The signal representation can be further simplified using Laurent's approximation [12, 18] to reduce

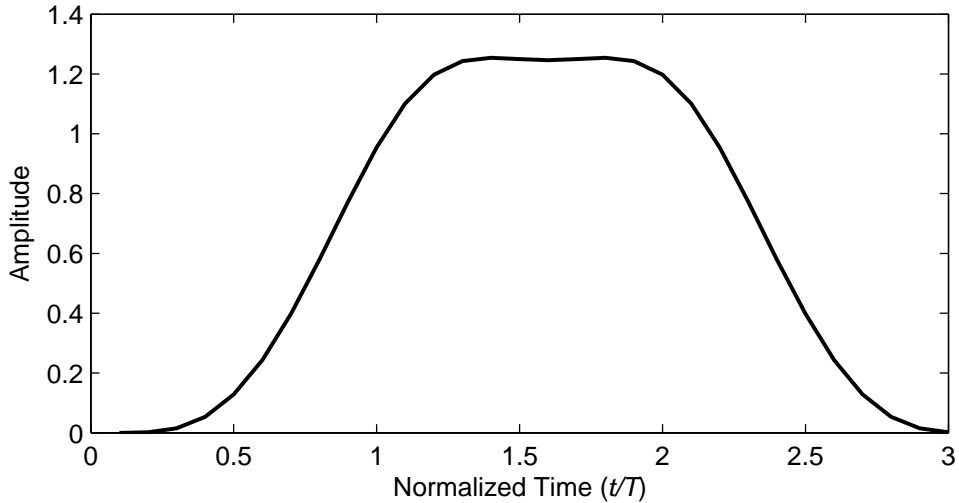


Figure 2.7. The main pulse $p(t)$.

the complexity of the receiver design (refer to Appendix V)

$$s(t; \boldsymbol{\alpha}) \cong \tilde{s}(t; \boldsymbol{\alpha}) = \sum_n b[n]p(t - nT) \quad (2.17)$$

where

$$b[n] = \exp\left(j\pi h \sum_{l=-\infty}^n a[l]\right). \quad (2.18)$$

We would like to mention here that $b[n]$ here is same as $b_0[n]$. We have dropped the subscript for simplicity. We use main PAM pulse $p(t)$ shown in Figure 2.7 which is similar to $c_0(t)$ for the best CPM signal approximation. The main PAM pulse $p(t)$ is chosen to minimize the mean square error (MSE) between (7.21) and (7.20) [12]. The shape of the pulse $p(t)$ depends on the modulation index h .

2.4 Summary

In this chapter we explained the CPM signal model. We also discussed the parameters for SOQPSK and PCM/FM. We explained the 4-state and 2-state trellis diagrams for SOQPSK. We discussed the correspondence between phase states and trellis states and 2-state trellis based detector requires a decision feedback to calculate the CPM phase state. We also gave linear PAM decomposition model for the CPM signal.

Chapter 3

SOQPSK Detectors

Now that we have studied the signal model for SOQPSK, we explain the simplified detectors for SOQPSK in this chapter. We start with the received signal model and then show how simple detectors using PAM and PT techniques can be built [14,16,17,19]. Here in this chapter we will explain the procedure to calculate the branch metric update and the matched filters (MFs) required to implement the Viterbi Algorithm [10,11,20].

3.1 Received Signal Model

The received signal model is

$$r(t) = s(t; \boldsymbol{\alpha}) + w(t) \tag{3.1}$$

where $w(t)$ is complex-valued additive white Gaussian noise (AWGN) with single-sided power spectral density N_0 . Since the transmitted signal $s(t; \boldsymbol{\alpha})$ has memory, the optimal detector must perform maximum likelihood sequence detection (MLSD). This is efficiently implemented via the Viterbi algorithm (VA). In the

following discussion, the estimated and hypothesized values of a quantity w are referred to as \hat{w} and \tilde{w} respectively. Also, \hat{w} and \tilde{w} can assume the same values as w itself.

The VA operates on the trellis diagram. Hypothetically speaking, it is possible that the transmitted signal is in any one of the allowable states. The likelihood that the transmitter is in a given hypothetical state \tilde{S}_n at a given time step n is quantified by the *cumulative metric* $\lambda_n(\tilde{S}_n)$. A cumulative metric is maintained for each state in the trellis. These metrics are extended along the branches from starting states \tilde{S}_n to ending states \tilde{E}_n via the update

$$\lambda_{n+1}(\tilde{E}_n) = \lambda_n(\tilde{S}_n) + z(n, [\tilde{a}_n, \tilde{S}_n]) \quad (3.2)$$

where $z(n, [\tilde{a}_n, \tilde{S}_n])$ is the *branch metric increment* and is a function of the starting state \tilde{S}_n and the branch symbol \tilde{a}_n ; $[\tilde{a}_n, \tilde{S}_n]$ is the *branch vector*. In the case of SOQPSK, there are two branches that merge into each ending state \tilde{E}_n . The branch with the maximum metric is declared as the *survivor* and its metric is stored for later use in the next round of updates.

This general VA framework will be used for both the 4-state and 2-state SOQPSK detectors. Before doing this, we will summarize how partial-response SOQPSK-TG is handled at the receiver as if it were a full-response waveform.

3.2 Branch Metric Increment Using Pulse Truncation

One technique for reducing the complexity of SOQPSK-TG at the receiver is known as pulse truncation (PT) [3, 25]. This approach stems from the fact that frequency pulses which are long and smooth are oftentimes near-zero for a

significant portion of their duration. This is clearly the case for $f_{\text{TG}}(t)$ in Fig. 2.1. Using these arguments, we base the detector on a frequency pulse which has been truncated to a duration of one symbol time (full-response). The detector uses a *phase* pulse instead of a *frequency* pulse 3.4, so we translate these arguments accordingly and obtain a modified phase pulse

$$q_{\text{PT}}(t) = \begin{cases} 0, & t < 0 \\ q(t + (L - 1)T/2), & 0 \leq t \leq T \\ 1/2, & t > T. \end{cases} \quad (3.3)$$

Note that the phase pulse in (3.3) is defined for all values of t ; however, its time-varying portion has been shortened by a total of $(L - 1)T$ and is restricted to the interval $[0, T]$. The truncation is centered such that half is applied to the beginning of the pulse and half to the end. Since $q_{\text{PT}}(t)$ has variations only in the time interval $[0, T]$ it behaves like a full-response pulse.

The truncated pulse can be used in a standard CPM-type branch metric increment [2]

$$z_{\text{PT}}(n, [\tilde{a}_n, \tilde{S}_n]) \triangleq \text{Re} \left[e^{-j\tilde{\theta}_{n-1}} \int_{nT}^{(n+1)T} r(t + (L-1)T/2) e^{-j2\pi h \tilde{a}_n q_{\text{PT}}(t-nT)} dt \right] \quad (3.4)$$

The hypothesized branch vector $[\tilde{a}_n, \tilde{S}_n]$ has a one-to-one correspondence with a hypothesized ternary symbol \tilde{a}_n and a hypothesized CPM phase state $\tilde{\theta}_{n-1}$, as shown in Fig. 2.3 and equation (2.13), respectively. There are three complex-valued matched filter (MF) outputs needed to implement (3.4) (one for each possible value of the ternary \tilde{a}_n).

While the notation in (3.3) and (3.4) is valid for SOQPSK-MIL and SOQPSK-

TG, in the case of SOQPSK-MIL ($L = 1$) the pulse $q_{\text{MIL}}(t)$ is already full-response and no truncation takes place. For this reason, we refer to (3.4) as the “MF metric” in the case of SOQPSK-MIL since it is in fact the *optimal* CPM-type metric. In the case of SOQPSK-TG, we refer to (3.4) as the “PT metric” and it results in *near-optimal* performance, as discussed in Sections 4 and 4.4.

3.3 Branch Metric Increment Using the PAM

Representation

Using the PAM representation of ternary CPM [16], the right-hand side of (2.1) can be written as

$$s(t; \boldsymbol{\alpha}) = \sum_n \sum_{k=0}^{R-1} b_k[n] g_k(t - nT), \quad R = 2 \cdot 3^{L-1} \quad (3.5)$$

which is simply a linear combination of R pulses $g_k(t)$ that are modulated by *pseudo-symbols* $b_k[n]$. The pseudo-symbols are derived from the original data symbols α_i by a nonlinear mapping.

For the present case of SOQPSK, an important property of the PAM technique is the following: when (3.5) is approximated with the first two terms in the inner summation, i.e.

$$s(t; \boldsymbol{\alpha}) \approx \sum_n \sum_{k=0}^1 b_k[n] g_k(t - nT), \quad (3.6)$$

the pseudo-symbols that remain, $b_0[n]$ and $b_1[n]$, can be described by the full-response trellis in Fig. 2.3. Thus, the PAM approximation in (3.6) can be used to realize 4-state detectors for partial-response SOQPSK (and SOQPSK-TG in particular). The PAM approximation in (3.6) is composed of two pulses $g_0(t)$ and

$g_1(t)$ given as

$$g_k(t) = \begin{cases} c_0^2(t), & k = 0 \\ c_0(t)c_0(t+T), & k = 1. \end{cases} \quad (3.7)$$

The pulse $c_0(t)$ is given by

$$c_0(t) = \prod_{i=0}^{L-1} u(t+iT) \quad (3.8)$$

where

$$u(t) = \begin{cases} \sin(2\pi hq(t))/\sin(\pi h), & 0 \leq t < T \\ \sin(\pi h - 2\pi hq(t-LT))/\sin(\pi h), & LT \leq t < 2T \\ 0, & \text{otherwise.} \end{cases} \quad (3.9)$$

The PAM-based branch metric increment is given by [19]

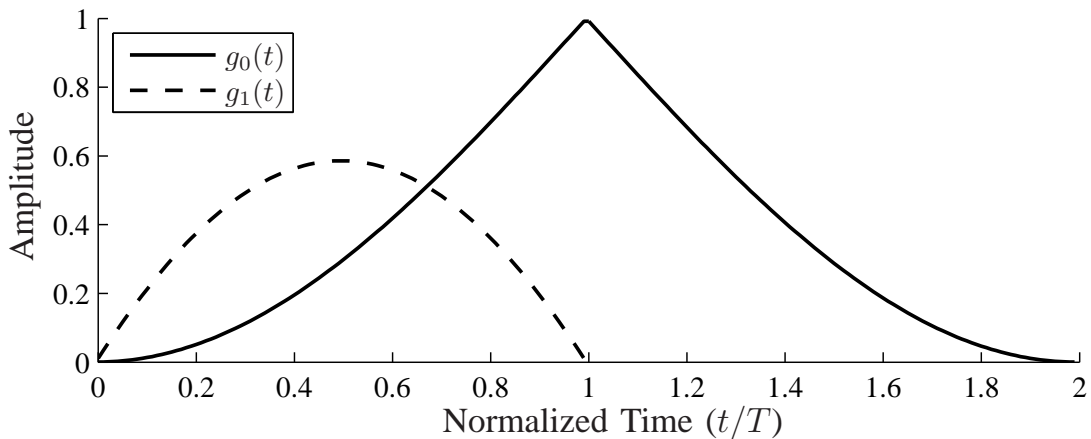
$$z_{\text{PAM}}(n, [\tilde{a}_n, \tilde{S}_n]) = \text{Re} \left[e^{-j\tilde{\theta}_{n-1}} \sum_{k=0}^1 y_k(n) [\beta_k(\tilde{a}_n)]^* \right] \quad (3.10)$$

where $(\cdot)^*$ is the complex conjugate. The pseudo-symbols $\beta_k(\cdot)$ in (3.10) are listed in Table 3.1. The sampled matched MF output is

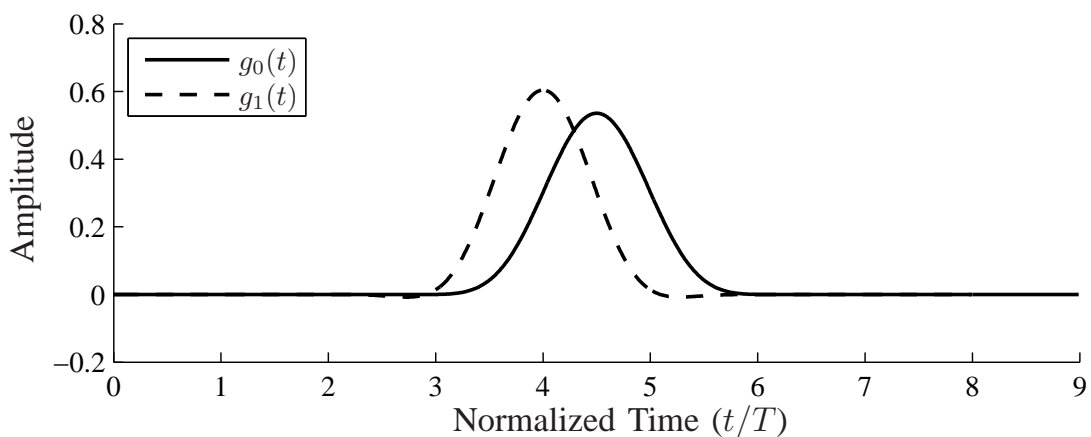
$$y_k(n) = \int_{nT}^{(n+L+1-k)T} r(t)g_k(t-nT) dt. \quad (3.11)$$

The hypothesized branch vector $[\tilde{a}_n, \tilde{S}_n]$ has a one-to-one correspondence with \tilde{a}_n and $\tilde{\theta}_{n-1}$, as discussed before. In this case, \tilde{a}_n corresponds to a row in Table 3.1. The PAM pulses $g_0(t)$ and $g_1(t)$ are shown in Fig. 3.1(a) for SOQPSK-MIL and Fig. 3.1(b) for SOQPSK-TG.

Here again, the notation in (3.10) is valid for SOQPSK-MIL and SOQPSK-TG.



(a)



(b)

Figure 3.1. The two principal pulses for the PAM representation of (a) SOQPSK-MIL and (b) SOQPSK-TG.

In the case of SOQPSK-MIL, the exact PAM representation has only $R = 2$ terms so the approximation in (3.6) turns out to be exact. Thus, (3.10) is *optimal* in the case of SOQPSK-MIL. In the case of SOQPSK-TG, the exact PAM representation has $R = 4374$ terms, so (3.6) is truly an approximation and (3.10) results in a *near-optimal* detector, as discussed in the next chapter.

Table 3.1. The relationship between the ternary branch symbol α_n , and the pseudo-symbols $\beta_k(\alpha_n)$ for SOQPSK.

α_n	$\beta_0(\alpha_n)$	$\beta_1(\alpha_n)$
-1	$\exp\{-j\pi/2\} = -j$	$\exp\{-j\pi/4\} = \frac{\sqrt{2}}{2}(1-j)$
0	1	$\cos(\pi/4) = \frac{\sqrt{2}}{2}$
1	$\exp\{j\pi/2\} = j$	$\exp\{j\pi/4\} = \frac{\sqrt{2}}{2}(1+j)$

3.4 2-State Detectors for SOQPSK

In this thesis we develop 2-state detectors for SOQPSK for the first time. As mentioned earlier, the difficulty with the two state trellis in Fig. 2.4 is that a one-to-one correspondence between the sign state \mathcal{S}_n and the CPM phase state θ_{n-1} does not exist. Thus, when given the branch vector $[\tilde{a}_n, \tilde{\mathcal{S}}_n]$, there is not enough information to compute the branch metric updates in (3.4) and (3.10). This problem is overcome by using decision feedback on a per-survivor basis (i.e. Per Survivor Processing (PSP) [21]).

As mentioned above, at the end of each time step, a surviving branch is declared at each ending state \tilde{E}_n in the trellis. We use $\hat{\alpha}_n(\tilde{E}_n)$ to denote the symbol associated with the surviving branch at each ending state \tilde{E}_n . In the modified VA, a *cumulative phase* $\hat{\theta}_{n-1}(\tilde{\mathcal{S}}_n)$ is maintained for each state $\tilde{\mathcal{S}}_n$ in the trellis, in addition to the above-mentioned cumulative metric $\lambda_n(\tilde{\mathcal{S}}_n)$. Once the survivors have been declared, the cumulative phase for each ending state is updated via the recursion

$$\hat{\theta}_n(\tilde{E}_n) = \left[\hat{\theta}_{n-1}(\tilde{\mathcal{S}}_n) + \pi h \hat{\alpha}_n(\tilde{E}_n) \right] \text{ mod } 2\pi. \quad (3.12)$$

As it turns out, in the case of the 4-state detector the cumulative phase $\hat{\theta}_{n-1}(\tilde{\mathcal{S}}_n)$ is identical to the phase state $\tilde{\theta}_{n-1}$ provided the four cumulative phases are initialized according to (2.13) at the start of the algorithm. This is equivalent

to saying that, given the proper initialization, the two branches merging at each ending state in the 4-state trellis will result in the same value for the cumulative phase. This is true by definition of the phase state in (2.4) and the cumulative phase in (3.12). Thus, decision feedback does not introduce any sub-optimality compared to the 4-state detectors.

In the case of the 2-state detector, using $\hat{\theta}_{n-1}(\tilde{S}_n)$ instead of $\tilde{\theta}_{n-1}$ does make the detector suboptimal, but it is a necessary step in order to implement the detector in the first place. The impact of decision feedback on the performance of the 2-state detectors is studied in the next chapter.

3.5 Summary

In this chapter we discussed the PAM based detectors for SOQPSK. We also explained the second approach we have implemented for SOQPSK detection i.e. PT. We showed how the *phase state* can be calculated for a 2-state trellis detector using decision feedback.

Chapter 4

SOQPSK Performance Analysis

The bit-error probability of SOQPSK in AWGN is described using error events and minimum distance concepts. The normalized squared Euclidean distance of CPM is [2]

$$d^2 = \frac{\log_2 M_{\text{info}}}{2T} \int |s(t; \mathbf{\alpha}_{\text{Tx}}) - s(t; \mathbf{\alpha}_{\text{Rx}})|^2 dt \quad (4.1)$$

where $\log_2 M_{\text{info}}$ is the number of bits per symbol (for SOQPSK we have $M_{\text{info}} = 2$).

4.1 Minimum Distance Error Event

The minimum distance error event for the 4-state SOQPSK detectors is where the transmitted and received *bit* sequences satisfy

$$\begin{aligned} \mathbf{a}_{\text{Tx}} &= \dots, a_{e-1}, a_e, a_{e+1}, a_{e+2}, a_{e+3}, \dots \\ \mathbf{a}_{\text{Rx}} &= \dots, a_{e-1}, \bar{a}_e, a_{e+1}, \bar{a}_{e+2}, a_{e+3}, \dots \end{aligned} \quad (4.2)$$

In words, this is a double *bit* error event where the first error occurs at some arbitrary bit location a_e and the second error occurs with bit a_{e+2} . When $a_{e+1} = 0$,

the precoded symbol sequences satisfy $\pm\gamma_0$, where

$$\gamma_0 = \boldsymbol{\alpha}_{\text{Tx}} - \boldsymbol{\alpha}_{\text{Rx}} = \dots, 0, -1, 0, +1, 0, \dots \quad (4.3)$$

and a squared distance of d_0^2 results (refer to Appendix IV for an e.g to calculate the squared distance). When $a_{e+1} = 1$, the precoded symbol sequences satisfy $\pm\gamma_1$, where

$$\gamma_1 = \boldsymbol{\alpha}_{\text{Tx}} - \boldsymbol{\alpha}_{\text{Rx}} = \dots, 0, -1, -2, +1, 0, \dots \quad (4.4)$$

and a squared distance of d_1^2 results. These cases are easily verified by examining the 4-state trellis in Fig. 2.3.

4.2 Additional Error Event for 2-State Detectors

For the 2-state detectors, an additional error event is introduced where the transmitted and received *bit* sequences satisfy

$$\begin{aligned} \boldsymbol{a}_{\text{Tx}} &= \dots, a_{e-1}, a_e, a_{e+1}, a_{e+2}, \dots \\ \boldsymbol{a}_{\text{Rx}} &= \dots, a_{e-1}, \bar{a}_e, \bar{a}_{e+1}, a_{e+2}, \dots \end{aligned} \quad (4.5)$$

In words, this is a double *bit* error event where the first error occurs at some arbitrary bit location a_e and the second error occurs with the following bit a_{e+1} . In this case, it is easily verified from Fig. 2.3 that the precoded symbol sequences satisfy $\pm\gamma_2$, where

$$\gamma_2 = \boldsymbol{\alpha}_{\text{Tx}} - \boldsymbol{\alpha}_{\text{Rx}} = \dots, 0, +1, +1, 0, \dots \quad (4.6)$$

We denote the squared distance in this case by d_2^2 .

4.3 Probability of Bit Error

The PT and PAM approximations discussed earlier result in *mismatched detectors* [3, 25], i.e. the detector is no longer matched to the transmitted signal. The mismatched detectors require the analysis to be more intricate. The minimum distance error event is still given by (4.2), and the 2-state detectors still have the additional error event (4.5), but instead of having a single distance value in each case, say d_0^2 , we get a *set* of distance values, $\{d_{0,l}^2\}$. For example, with SOQPSK-TG the optimal (fully matched) detector has $d_0^2 = 1.60$ (refer to Appendix IV). When the 4-state PT detector is used, the distance is slightly influenced by the values of the bits surrounding the error event on each side, $\{a_{e-k}\}_{k=1}^3$ and $\{a_{e+k}\}_{k=3}^5$. This results in a set of distance values $\{d_{0,l}^2\}_{l=0}^{63}$ that are clustered around the value $d_0^2 = 1.60$ and range from 1.38 to 1.77. The methods for calculating these distances are discussed in [3, 17, 25]

Taking this behavior into account, the final expression for the union bound on the bit-error probability of the 4-state detectors is

$$P_{b,4} \leq \frac{1}{|d_{0,l}|_{\{d_{0,l}^2\}}} \sum Q\left(\sqrt{d_{0,l}^2 \frac{E_b}{N_0}}\right) + \frac{1}{|d_{1,l}|_{\{d_{1,l}^2\}}} \sum Q\left(\sqrt{d_{1,l}^2 \frac{E_b}{N_0}}\right) \quad (4.7)$$

where E_b/N_0 is the bit energy to noise ratio, $|\cdot|$ denotes the cardinality (number of elements) of a given set, and

$$Q(x) = \frac{1}{\sqrt{2\pi}} \int_x^\infty e^{-u^2/2} du. \quad (4.8)$$

For example, with the MF detector for SOQPSK-MIL, we have singleton sets of $d_0^2 = 1.73$ and $d_1^2 = 2.36$, so (4.7) simplifies to a summation of only two terms. In

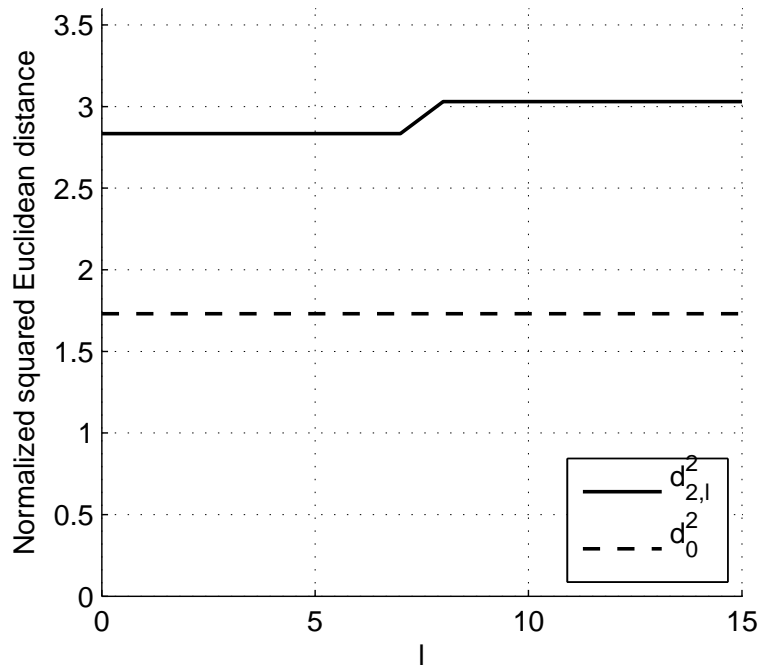


Figure 4.1. Range of distances for 2-state SOQPSK-MIL PAM-based detector.

the case of SOQPSK-TG, (4.7) contains the 128 terms in $\{d_{0,l}^2\}_{l=0}^{63}$ and $\{d_{1,l}^2\}_{l=0}^{63}$ that are clustered around the values $d_0^2 = 1.60$ and $d_1^2 = 2.59$.

Table 4.1. Range of distance values in the set $\{d_{2,l}^2\}$ for the 2-state SOQPSK detectors.

Configuration	$\min_l \{d_{2,l}^2\}$	$\max_l \{d_{2,l}^2\}$
MIL-MF ($d_0^2 = 1.73$)	2.00	2.00
MIL-PAM ($d_0^2 = 1.73$)	2.83	3.03
TG-PT ($d_0^2 = 1.60$)	1.71	2.23
TG-PAM ($d_0^2 = 1.60$)	2.57	3.35

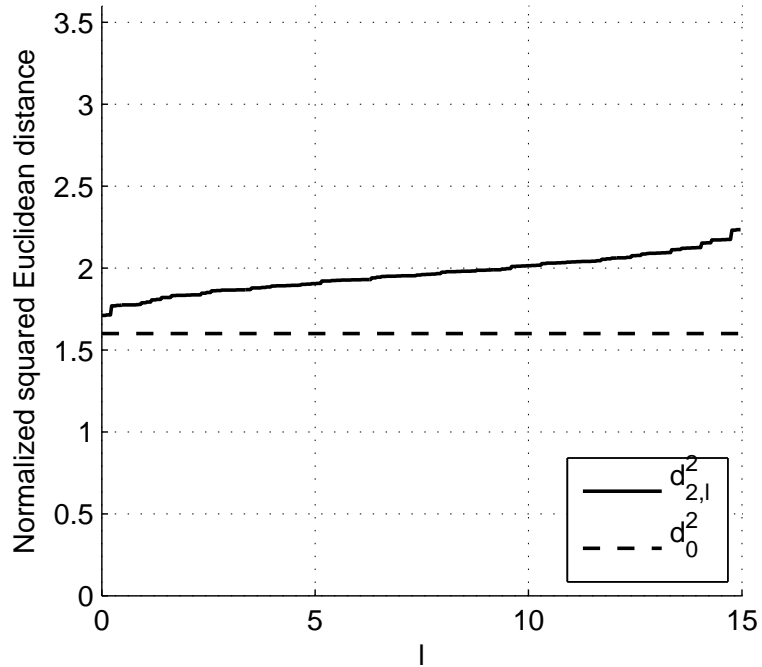


Figure 4.2. Range of distances for 2-state SOQPSK-TG PT-based detector.

4.4 Simulation Results

For the 2-state detectors, the bit-error probability is the same as that of the 4-state detectors but with an additional summation, i.e.

$$P_{b,2} \leq P_{b,4} + \frac{1}{|d_{2,l}|} \sum_{\{d_{2,l}^2\}} Q\left(\sqrt{d_{2,l}^2 \frac{E_b}{N_0}}\right). \quad (4.9)$$

Since (4.7) and (4.9) differ only by the terms introduced by the additional merger in (4.5), the values in $\{d_{2,l}^2\}$, which are summarized in Table 4.1, are the key to quantifying the performance of the 2-state detectors relative to the 4-state detectors. The first observation from Table 4.1 is that, with all four of the 2-state configurations, the distances in $\{d_{2,l}^2\}$ exceed the value of d_0^2 , i.e. the minimum distance is *not worsened* by the 2-state detectors. This means that the 2-state

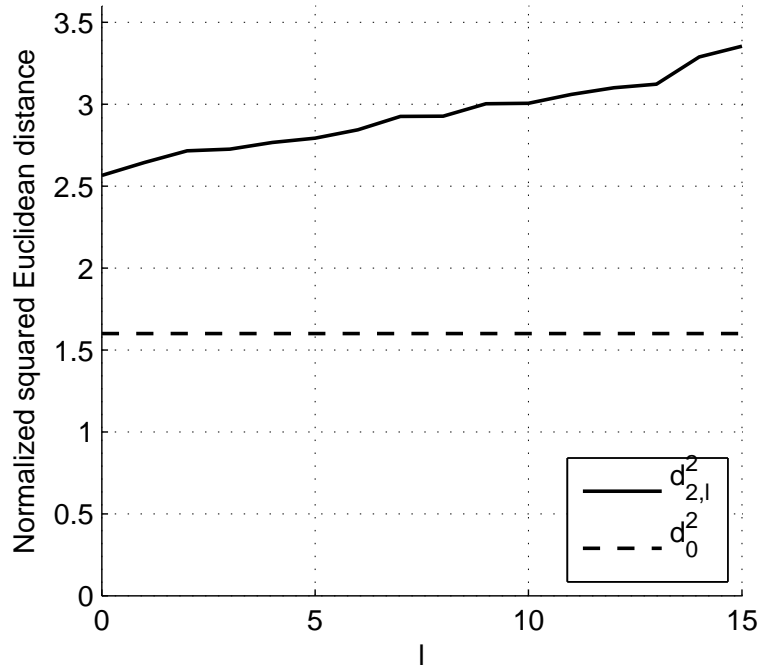


Figure 4.3. Range of distances for 2-state SOQPSK-TG PAM-based detector.

detectors each have a performance that is asymptotically equivalent (large E_b/N_0) to their 4-state counterpart. The second observation from Table 4.1 is that the PAM-based detectors have values in $\{d_{2,l}^2\}$ that are far greater than d_0^2 , while the MF and PT detectors have values that are relatively close to d_0^2 ; thus, even for moderate ranges of E_b/N_0 we would expect the PAM-based detectors to have performance identical to the 4-state detectors, while the MF and PT detectors should have minor losses for moderate values of E_b/N_0 . Figures 4.1 and 4.3 support the fact that, for the PAM-based detectors the range of distances are far away from the minimum distance, hence has little effect on the performance. Where as referring to Figure 4.2 we can see that the distance values for SOQPSK-TG PT remains closer to the minimum distance, hence having a greater effect on performance resulting in minor losses. We present the simulation results next to

support the performance of the simplified detectors.

There are two modulation types (SOQPSK-MIL and SOQPSK-TG), two trellis sizes (2-state and 4-state), and two branch metric types (MF or PT, and PAM) that have been discussed above. This yields a total of eight detector configurations. Fig. 4.4 shows performance curves for the four SOQPSK-MIL configurations. In the low E_b/N_0 region of the figure, the 2-state union bounds given by (4.9) are not necessarily tight with respect to the simulation points (shown as points only, with no connections between points); however, the union bounds and the simulation points show close agreement rapidly as E_b/N_0 increases. Furthermore, the results anticipated in the previous section are confirmed. The 2-state PAM-based detector shows no observable degradation with the 4-state detector (across the entire simulation range of E_b/N_0), while the 2-state MF-based detector shows a slight performance degradation that narrows and is near zero at the large end of the simulated E_b/N_0 .

Fig. 4.5 shows performance curves for the four SOQPSK-TG configurations. As with the previous figure, the 2-state union bounds and the simulation points show close agreement rapidly as E_b/N_0 increases. Also, the 2-state PAM-based detector shows no observable degradation with the 4-state PAM detector, while the 2-state PT-based detector has a slight performance degradation with respect to the 4-state PT-based detector. Even in the 4-state case, the PAM technique has a 0.1 dB inherent advantage over the PT technique, as originally reported in [19].

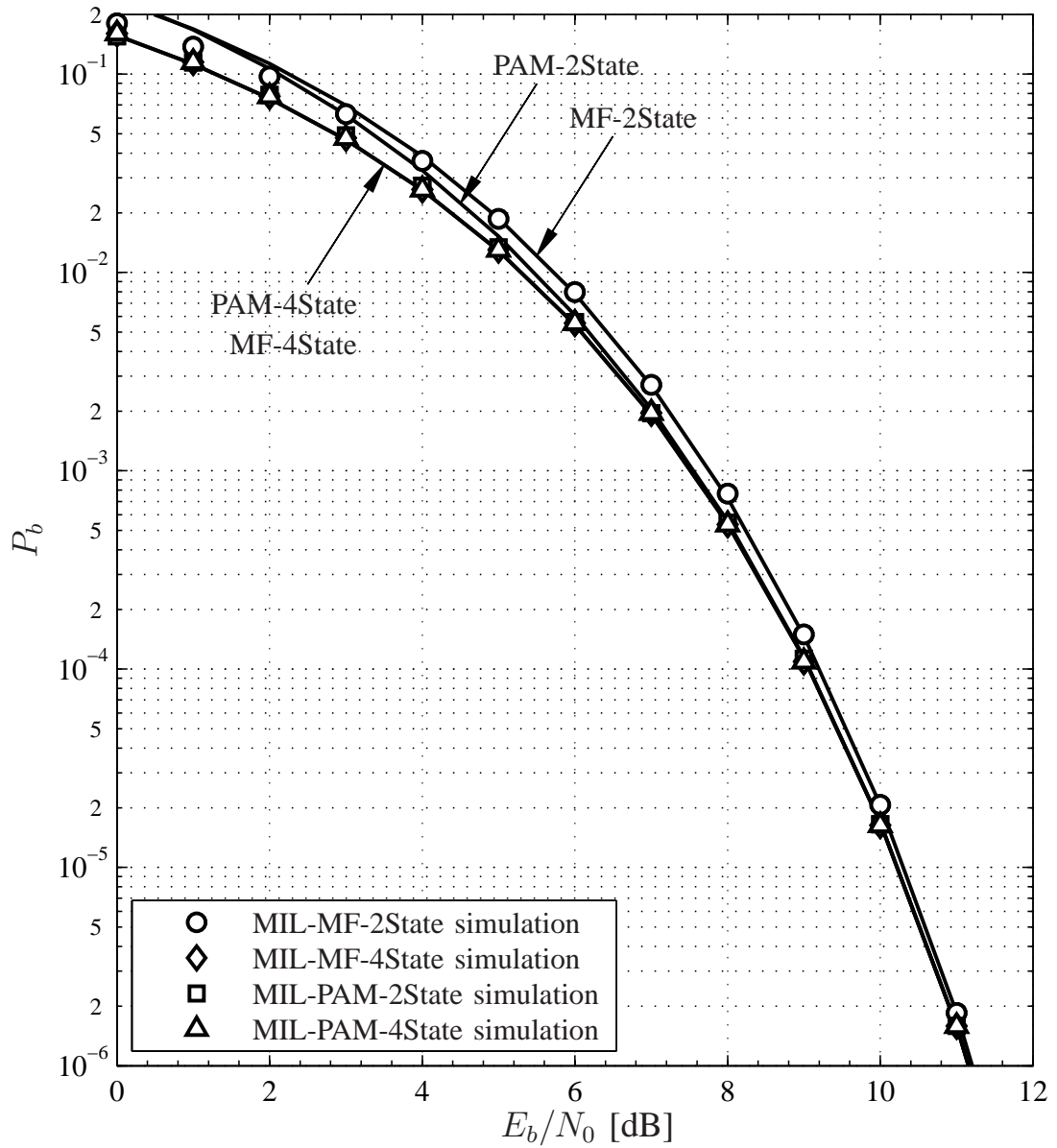


Figure 4.4. Performance of reduced-complexity detectors for SOQPSK-MIL.

4.5 Summary

We successfully built the 2-state PAM and PT based detectors for SOQPSK-MIL and SOQPSK-TG.

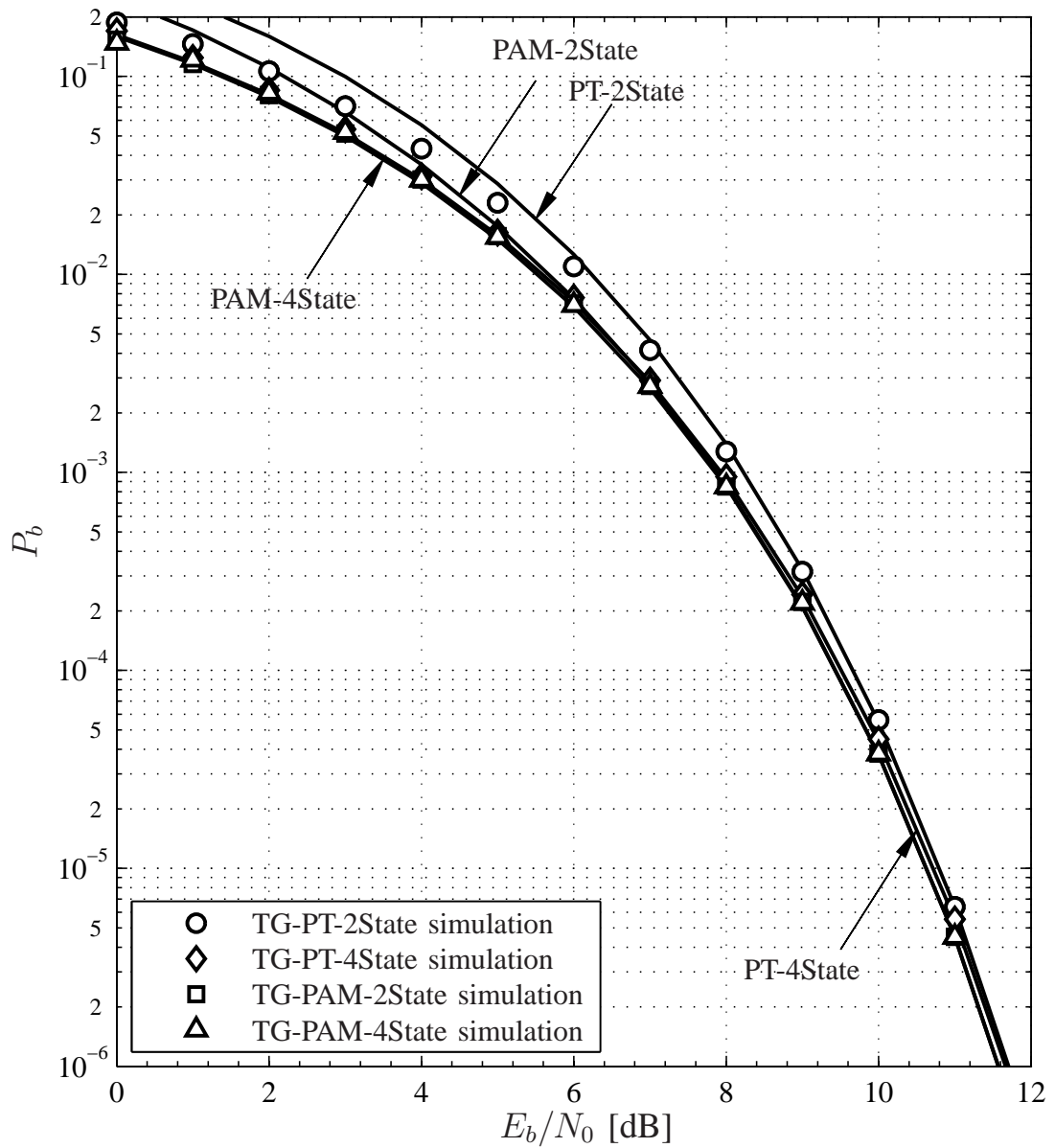


Figure 4.5. Performance of reduced-complexity detectors for SOQPSK-TG.

Chapter 5

PCM/FM Detection

Now that we have given the SOQPSK detectors and their performance analysis, we will study PCM/FM receiver design and then the performance of the detectors [4]. The signal model and the equivalent PAM decomposition for PCM/FM were explained in section 2.3. The PAM approximation helps to derive low-complexity detectors.

5.1 Receiver Design

The received signal is represented using

$$r(t) = s(t; \boldsymbol{\alpha}) + w(t) \quad (5.1)$$

where $w(t)$ is additive white Gaussian noise (AWGN) with power spectral density N_0 .

Our main goal in working with PCM/FM detectors is to develop a simplified detector with no states. We will also compare the performance of 2 and 4 state detectors with that of 0-state detector. As mentioned earlier, with PAM decom-

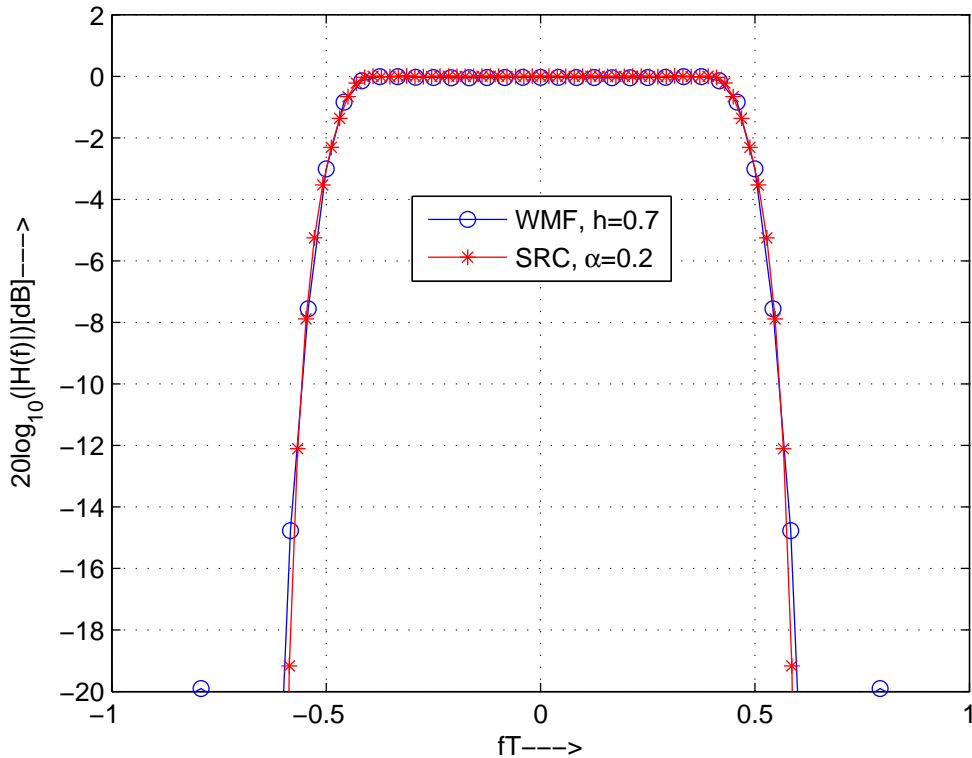


Figure 5.1. Magnitude frequency response for WMF $H_{\text{WMF}}(f)$ with $h = 0.7$ and for SRC filter with roll-off factor of 0.2.

position the nonlinear CPM signal is transformed into a linear modulation over an intersymbol-interference (ISI) channel. To get rid of the ISI we resort to a Decision Feedback Equalizer (DFE) [6]. We explain the DFE as we move on in this chapter.

The receiver input filter is desired to have a square-root Nyquist frequency response [20] to achieve the ISI suppression. A whitened matched filter (WMF) matches this condition. Applying the PAM approximation (7.21) and received signal model (5.1), the frequency response of the whitening matched filter (WMF) can be written as

$$H_{\text{WMF}}(f) = \frac{P(f)}{\sqrt{\sum_{n=-\infty}^{\infty} |P(f - n/T)|^2}} \quad (5.2)$$

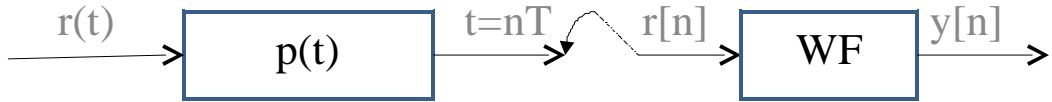


Figure 5.2. Receiver design for PCM/FM using WF.

where $P(f)$ is the Fourier transform of the main PAM pulse $p(t)$. Since $p(t)$ depends on the modulation index h , the WMF depends on the modulation index as well. Recall from Chapter 1 that typical PCM/FM transmitters have some variation in their modulation index due to antiquated analog circuitry. In Figure 5.1 we show the response of an off-the-shelf square-root cosine (SRC) filter with impulse response $h_{\text{SRC}}(t)$. We note that the WMF and SRC filters have similar frequency response. We can use the SRC filter as the receiver filter to avoid the variations of WMF with h . However we discuss both of these approaches here.

5.2 Reduced State Sequence Detection (RSSD)

The overall receiver design with the whitening filter is shown in Figure 5.2. The received signal is passed through the main pulse $p(t)$ and sampled at the symbol-rate, i.e.

$$r[n] = r(t) * p(t)|_{t=nT} = \sum_{l=0}^{q_{h_c}} h_c[l]b[n-l] + w[n] \quad (5.3)$$

where $h_c[n]$ is the discrete-time channel impulse response

$$h_c[n] = p(t) * p(t)|_{t=nT}, \quad 0 \leq n \leq q_{h_c} \quad (5.4)$$

of order q_{h_c} . The *pseudo-symbols* $b[n]$ were discussed in Equations (2.15) and (7.20). The noise $w[n]$ in (5.3) is correlated due to the shape of $p(t)$. Then the sampled received signal is passed through the whitening filter (WF) to make the resulting noise uncorrelated. The WF is given below

$$\text{WF}(n) = \frac{1}{31.5336} \left[\frac{1}{1.8226} (-0.5487)^{(n)} - \frac{1}{33.3562} (-0.03)^{(n)} \right] \quad (5.5)$$

where $-8 \leq n \leq 0$. We developed the WF for PCM/FM using the main PAM pulse $p(t)$ with the modulation index being the nominal PCM/FM value $h = 7/10$. We will explain the construction of the whitening filter in Appendix III. It can be noted that changing the pulse shape and the modulation index results in the change of the whitening filter shown above. Equation (5.3) gives a very good approximation of the received signal. After passing the sampled received signal through the whitening filter the received sequence $y[n]$ looks like

$$y[n] = r[n] * \text{WF}[n] = \sum_{l=0}^{q_{h_0}} h_0[l] b[n-l] + v[n] \quad (5.6)$$

where the overall impulse response is given by

$$h_0[n] = h_c[n] * \text{WF}[n] \quad (5.7)$$

of order $q_{h_c} = 2$.

The overall receiver design with SRC filter is shown in Figure 5.3. Using

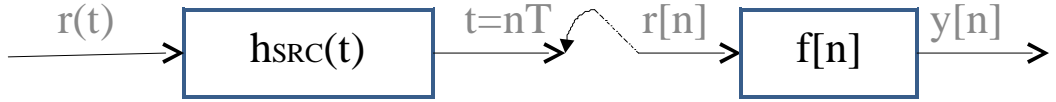


Figure 5.3. Receiver design for PCM/FM using $h_{\text{SRC}}(t)$.

the second approach with the SRC filter, sampling $r(t)$ at symbol-rate yields the approximation

$$r[n] = r(t) * h_{\text{SRC}}(t)|_{t=nT} = \sum_{l=0}^{q_{h_c}} h_c[l]b[n-l] + w[n] \quad (5.8)$$

where the discrete-time channel impulse response is given by

$$h_c[n] = p(t) * h_{\text{SRC}}(t)|_{t=nT}, \quad 0 \leq n \leq q_{h_c} \quad (5.9)$$

here $w[n]$ is filtered additive white Gaussian Noise (AWGN). The overall impulse response in this case is given by

$$h_0[n] = h_c[n] * f[n] \quad (5.10)$$

where $f[n]$ is the feedforward filter (FFF) for the minimum mean-square error (MMSE) decision feedback equalizer (DFE) [6]. The implementation of $f[n]$ is explained in [6]. This filter gives a minimum-phase overall impulse response to obtain a high performance with RSSD. The filtered received sequence $y[k]$ is given

by

$$y[n] = r[n] * f[n] \quad (5.11)$$

The trellis state can be defined as a vector $\tilde{\mathbf{a}}[n] = [\tilde{a}[n] \dots \tilde{a}[n - n_s + 1]]$ of n_s hypothetical data symbols $\tilde{a}[n]$. Then we have 2^{n_s} states, where n_s is a design parameter. We also have a vector $\hat{\mathbf{b}}[n] = [\hat{b}[n - n_s] \dots \hat{b}[n - q_{h_0} + 1]]$ associated with each state ($\hat{\mathbf{b}}[n] = \hat{b}[n - n_s]$ if $n_s \geq q_{h_0}$). We apply decision feedback on a per-survivor basis to determine the symbols $\hat{b}[k]$.

We use a trellis diagram with 2^{n_s} states. Since we are implementing the VA, we compute the branch metric using

$$z\left(n, \left[\tilde{\mathbf{a}}[n-1], \tilde{a}[n]\right]\right) = \left|d[n] - \sum_{l=0}^{n_s} h_0[l] \tilde{b}[n-l]\right|^2 \quad (5.12)$$

where

$$d[n] = y[n] - \sum_{l=n_s+1}^{q_{h_0}} h_0[l] \hat{b}[n-l] \quad (5.13)$$

and

$$\tilde{b}[n-l] = \hat{b}[n - n_s - 1] \exp\left(j\pi h \sum_{k=n-n_s}^{n-1} \tilde{a}[k]\right) \quad (5.14)$$

for $0 \leq l \leq n_s$. For $n_s = 0$ the decision rule simplifies to

$$\hat{a}[n] = \arg \max_{\tilde{a}[n]} \operatorname{Re} \left\{ d^*[n] \hat{b}[n-1] e^{j\pi h \tilde{a}[n]} \right\} \quad (5.15)$$

Then the cumulative metric is calculated as explained for SOQPSK. The VA has already been discussed in detail while discussing the SOQPSK results.

5.3 Summary

Here in this chapter we explained the simplified PCM/FM signal model. We explained the reduced complexity PAM based detectors for PCM/FM using two approaches, the SRC filter and the whitening filter. We also explained the VA for PCM/FM detection. We explained the special case of PCM/FM detector the number of states is reduced to zero.

Chapter 6

PCM/FM Results

The bit-error rate (BER) of the optimal detector for PCM/FM is given by

$$P_b \approx Q\left(\sqrt{d^2 \frac{E_b}{N_0}}\right) \quad (6.1)$$

where $d^2 = 2.60$ (BPSK has $d^2 = 2.0$). A distance greater than 2.0 is achieved because of the coding gain and memory involved in CPM). The minimum distance error event for PCM/FM detectors is where the transmitted and received *symbol* sequences satisfy

$$\begin{aligned} \boldsymbol{\alpha}_{\text{Tx}} &= \dots, \alpha_{e-1}, \alpha_e, \alpha_{e+1}, \alpha_{e+2}, \dots \\ \boldsymbol{\alpha}_{\text{Rx}} &= \dots, \alpha_{e-1}, \bar{\alpha}_e, \bar{\alpha}_{e+1}, \alpha_{e+3}, \dots \end{aligned} \quad (6.2)$$

The symbol sequences satisfy $\pm\gamma$ (refer to Appendix IV), where

$$\boldsymbol{\gamma} = \boldsymbol{\alpha}_{\text{Tx}} - \boldsymbol{\alpha}_{\text{Rx}} = \dots, 0, -2, +2, 0, \dots \quad (6.3)$$

Figure 6.1 shows the performance for the PAM decomposition based detectors. We can see that as we increase the number of trellis states the BER approaches the optimal detector performance for large E_b/N_0 . 4-state detector using both SRC filter as well as the combination of $p(t)$ and WF gives a very good performance comparable to that of the optimal detector. By increasing the states of the trellis beyond 4, we did not find much of change in the performance of the detector. Also it makes the detector design more complicated and our aim is to design a simple detector. The optimal detector for PCM/FM used 20 states and 8 MFs. So we have discussed the performance of the detectors with 0 state, 2 states and 4 states. The 0-state detector has the obvious advantage of reduced complexity detection, but it suffers a 2 dB loss compared to the optimal detector. The 2-state detector gives a performance within 1 dB of the optimal detector. The performance of the 4-state detector is interesting. The complexity of the receiver is decreased with a performance close to the optimal detector. Also the 4-state detectors shows a 3–4 dB improvement compared to the FM demodulator.

6.1 Summary

We successfully developed 0, 2 and 4 state PAM based detectors for PCM/FM. We compared the performance of the reduced complexity PAM based detectors with the optimal detector (which has 20 states and uses 8 MFs). We see that 4-state detectors gives a performance that matches that of the optimal detectors for higher E_b/N_0 .

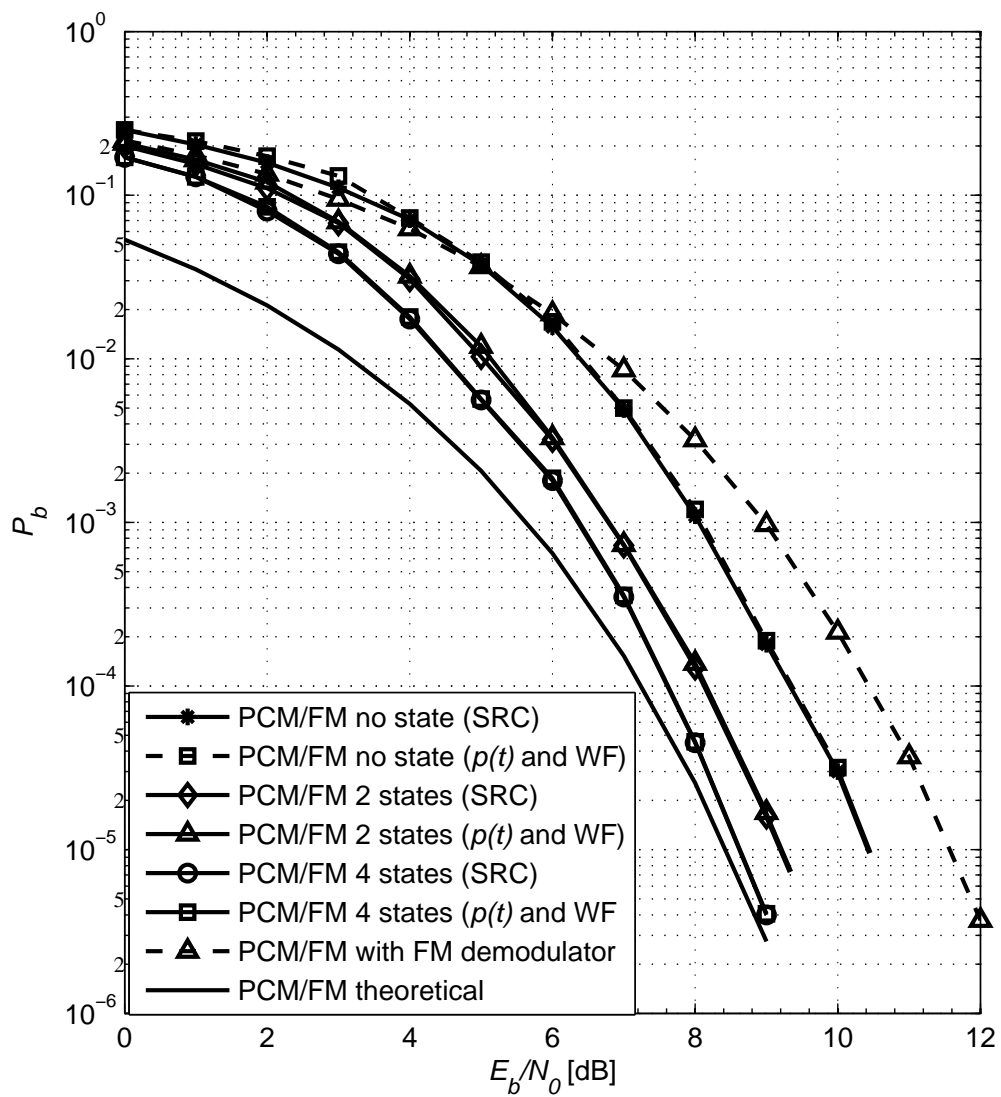


Figure 6.1. Performance of reduced-complexity detectors for PCM/FM.

Chapter 7

Conclusion

We have successfully developed reduced-complexity detectors for CPM signals, namely SOQPSK and PCM/FM using the PAM decomposition. Detectors using pulse truncation (PT) were also developed for SOQSPK signals. The performance analysis for SOQSPK show that 2-state detectors have performance that is asymptotically equivalent to their 4-state counterparts. This is a satisfying result due to the minimal 2-state level of complexity achieved by these detectors. We also successfully developed a 0-state detector for PCM/FM, but it did not perform as well as we hoped. It suffers a 2 dB loss compared to the optimal detector. The PAM decomposition based 2-state detector for PCM/FM gives good performance, it is 1 dB inferior to the optimal detector. But the 4-state trellis based detectors not only reduces the complexity of PCM/FM detectors but gives a near optimal performance, within 0.4 dB of the optimal detector. These simple detection schemes are applicable in settings where high-performance and low complexity are needed to meet restrictions on power consumption and cost.

7.1 Acknowledgment

This work was supported by the T&E/S&T Test Resource Management Center (TRMC) through the White Sands Contracting Office, contract number W9124Q-06-P-0337.

Appendix I - Optimal Detector Complexity

The modulation index for CPM is given by $h = k/p$. The state of a CPM signal is specified by

$$\sigma = [\theta_{n-L}, \alpha_{n-L+1}, \dots, \alpha_{n-1}]. \quad (7.1)$$

The number of states in the trellis is $p \cdot M^{L-1}$ from p cumulative phase states and M^{L-1} symbol combinations resulting from $(L - 1)$ -tuple. Since each state is associated with M possible branch symbols, the number of branches is $p \cdot M^L$. The number of matched filters is given by M^L . For e.g., PCM/FM has $p = 20$, $L = 2$ and $M = 2$. So we have $20 \cdot 2^{2-1} = 20$ trellis states and $2 \cdot 2^2 = 8$ MFs.

Appendix II - 2-state trellis

This proof is based on [15] The double differential encoder can be implemented as shown below. A *differentially encoded* sequence \mathbf{b} can be derived from the original data sequence \mathbf{a} by the operation [15]

$$b_n = a_n \oplus b_{n-1}, \quad \text{where } a_n, b_n \in \{0, 1\}, \quad n \in \{0, 1, 2, \dots\}. \quad (7.2)$$

If \mathbf{b} undergoes another differential encoding operation, we obtain

$$u_n = b_n \oplus u_{n-1} \quad (7.3)$$

and \mathbf{u} is double differentially encoded [24] sequence. Combining equations (7.2) and (7.3) we get

$$\begin{aligned} u_n &= \underbrace{a_n \oplus b_{n-1}}_{b_n} \oplus \underbrace{b_{n-1} \oplus u_{n-2}}_{u_{n-1}} \\ &= a_n \oplus u_{n-2} \end{aligned} \quad (7.4)$$

The double differential encoding rule in (7.4) can be summarized as “change phase on 1” since an input $a_n = 1$ causes the output value to change relative to the second previous value. A Boolean variable $u_n \in \{0, 1\}$ can be converted to antipodal

variable $\hat{u}_n \in \{\pm\}$ by

$$\hat{u}_n = 2u_n - 1. \quad (7.5)$$

or

$$-\hat{u}_n = (-1)^{u_n} \quad (7.6)$$

Also, the double differential encoder in (7.4) for antipodal bits is given as

$$\hat{u}_n = (-\hat{a}_n) \cdot \hat{u}_{n-2}, \quad \hat{a}_n, \hat{u}_n \in \{\pm\} \quad (7.7)$$

where ‘‘change phase on 1’’ rule holds good. For antipodal bits we have precoding operation as

$$\alpha_n = \frac{1}{2}(-1)^{n+1}\hat{u}_{n-1}(\hat{u}_n - u_{n-2}). \quad (7.8)$$

From equation (7.7) the above precoding equation reduces to

$$\begin{aligned} \alpha_n &= \frac{1}{2}(-1)^{n+1}\hat{u}_{n-1}(\underbrace{\hat{u}_n}_{-\hat{a}_n\hat{c}_{n-2}} - \hat{c}_{n-2}) \\ &= (-1)^{n+1} \underbrace{\frac{-\hat{a}_n - 1}{2}}_{-a_n} \hat{c}_{n-1}\hat{c}_{n-2} \\ &= (-1)^n a_n \hat{u}_{n-1}\hat{u}_{n-2} \end{aligned} \quad (7.9)$$

using (7.5) and (7.7) as well. Substituting (7.7) recursively

$$\begin{aligned} \hat{u}_{n-1}\hat{u}_{n-2} &= \prod_{i=-\infty}^{n-1} (-\hat{a}_i) \\ &= \prod_{i=-\infty}^{n-1} (-1)^{a_i} \\ &= (-1)^{\sum_{i=-\infty}^{n-1} a_i} \end{aligned} \quad (7.10)$$

Hence (7.8) becomes

$$\begin{aligned}\alpha_n &= (-1)^{n+\sum_{i=-\infty}^{n-1} a_i} a_n \\ &= (-1)^{S_n} a_n\end{aligned}\tag{7.11}$$

where the *sign state* S_n is given by

$$\begin{aligned}s_{n+1} &= (S_n + a_n + 1) \bmod 2 \\ &= (S_n + \alpha_n + 1) \bmod 2\end{aligned}\tag{7.12}$$

Appendix III - Whitening Filter Design

The received signal coming out of $p(t)$ has correlated noise. The whitening filter design is explained below. The sampled autocorrelation of the main pulse $p(t)$ is

$$p_d[n] = p(t) * p(t)|_{t=nT}. \quad (7.13)$$

The Z-transform of $p_d[n]$ can be represented as

$$P(Z) = \sum_{n=-L}^L p_d[n]z^{-n} \quad (7.14)$$

which can be expressed in factor form [20]

$$P(Z) = F(z) * F^*(z^{-1}) \quad (7.15)$$

where $F(z)$ is a polynomial of degree L having the roots $\rho_1, \rho_2, \dots, \rho_L$ and $F^*(Z^{-1})$ is a polynomial of degree L having the roots $1/\rho_1^*, 1/\rho_2^*, \dots, 1/\rho_L^*$. The desired whitening filter has a transform $1/F^*(z^{-1})$. We choose $1/F^*(z^{-1})$ that has anti-causal impulse response with poles of $X(Z)$ outside the unit circle. The filter in

our case with $L = 2$ reduces to

$$P(Z) = \sum_{n=-2}^2 p_d[n]z^{-n} = (a_2z^{-2} + a_1z^{-1} + 1)(a_2z^2 + a_1^*z + 1) \quad (7.16)$$

we use the assumption $|a| < 1$ and choose $F(z) = az^{-1} + 1$. We obtain a transversal filter with three taps $f_0 = 1$, $f_1 = a_1$ and $f_2 = a_2$.

For PCM/FM we can express the Z-transform of the autocorrelation of $p(t)$ as

$$P(Z) = (0.0164z^{-2} + 0.5786z^{-1} + 1)(0.0164z^2 + 0.5786z + 1) \quad (7.17)$$

giving $F(z) = 0.0164z^{-2} + 0.5786z^{-1} + 1$ and $F^*(z^{-1}) = 0.0164z^2 + 0.5786z^1 + 1$.

We need to find the filter $1/F^*(z^{-1})$. From 7.17 we have

$$1/F^*(z^{-1}) = \frac{1}{0.0164z^2 + 0.5786z^1 + 1} = \frac{1}{(z^1 + 33.3562)(z^1 + 1.8226)} \quad (7.18)$$

Using the residue theorem and taking inverse Z-transform the impulse response of the whitening filter can be approximated as

$$\text{WF}(n) = \frac{1}{31.5336} \left[\frac{(-0.5487)^n}{1.8226} - \frac{(-0.03)^n}{(33.3562)} \right] \quad (7.19)$$

The whitening filter can be tested by giving AWGN input and checking the autocorrelation of the noise coming out of WF. Figures 7.1, 7.2 and 7.3 show the autocorrelation of the main pulse $p(t)$ autocorrelation of noise after passing through the main pulse $p(t)$, and the finally the sampled autocorrelation output coming out of the WF. The autocorrelation being a delta function confirms the whitening property of the designed filter.

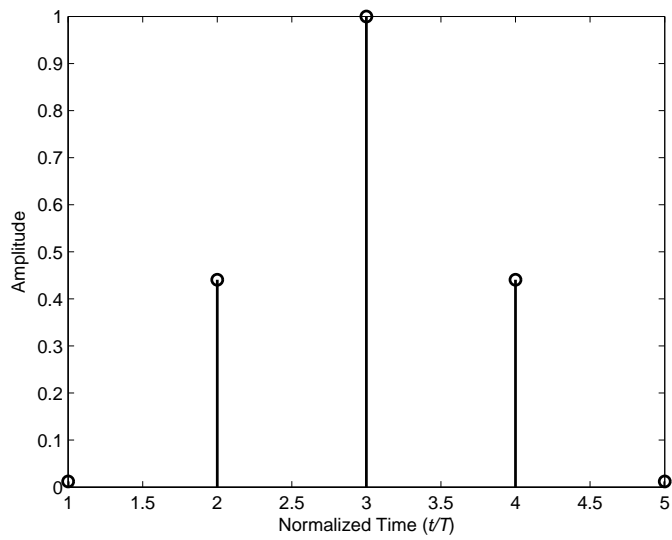


Figure 7.1. Autocorrelation of main pulse $p(t)$.

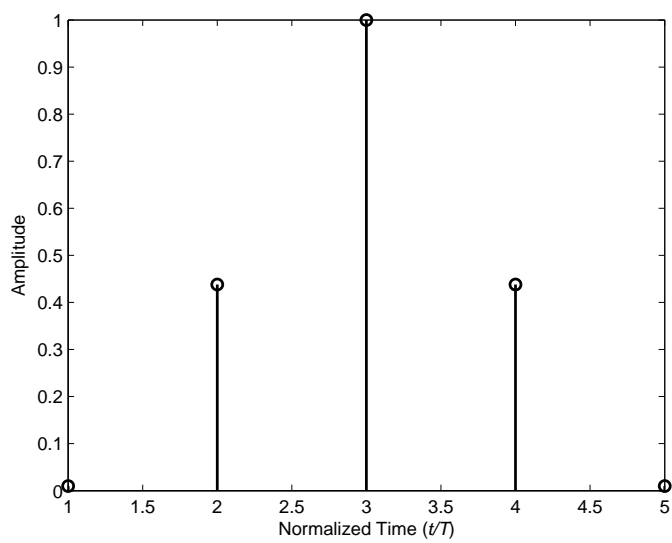


Figure 7.2. Autocorrelation of AWGN passed through $p(t)$.

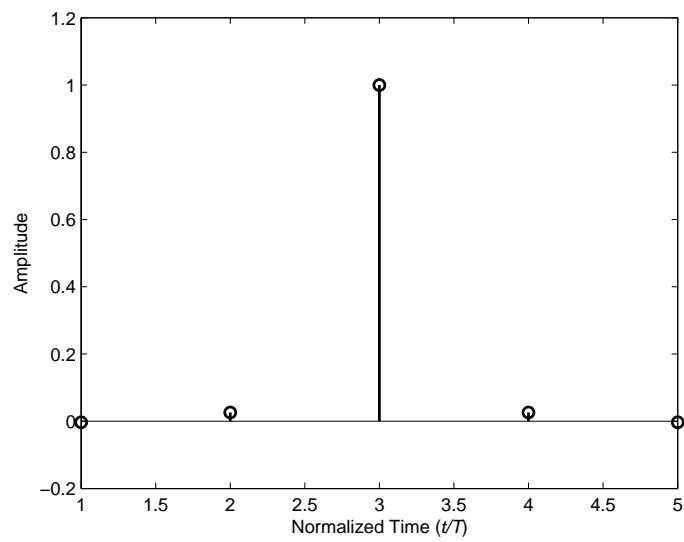


Figure 7.3. Autocorrelation of the sampled autocorrelation after passing through WF.

Appendix IV - Example to calculate the squared distance

For SOQPSK-MIL, we can find the minimum distance as given below(refer to Equations (2.1), (2.2), (4.1))

$$\begin{aligned}\boldsymbol{\alpha}_{\text{Tx}} &= [0 \ 0 \ 0] \\ \boldsymbol{\alpha}_{\text{Rx}} &= [1 \ 0 \ -1] \\ s(t; \boldsymbol{\alpha}_{\text{Tx}}) &= \exp(j\phi(t; \boldsymbol{\alpha}_{\text{Tx}})) \\ s(t; \boldsymbol{\alpha}_{\text{Rx}}) &= \exp(j\phi(t; \boldsymbol{\alpha}_{\text{Rx}}))\end{aligned}$$

where

$$\phi(t; \boldsymbol{\alpha}_{\text{Tx}}) = 2\pi \cdot \frac{1}{2}(0 + 0 + 0)$$

and

$$\begin{aligned}\phi(t; \boldsymbol{\alpha}_{\text{Rx}}) &= 2\pi \cdot \frac{1}{2}(q(t - T) + 0 - q(t - 2T)) \\ d_0^2 &= \frac{\log_2 2}{2T} \int (|s(t; \boldsymbol{\alpha}_{\text{Tx}}) - s(t; \boldsymbol{\alpha}_{\text{Rx}})|^2 dt\end{aligned}$$

gives $d_0^2 = 1.73$.

With precoded symbol sequences

$$\boldsymbol{\alpha}_{\text{Tx}} = [0 \ 0 \ 0]$$

$$\boldsymbol{\alpha}_{\text{Rx}} = [1 \ 0 \ -1]$$

we obtain a minimum distance of $d_0^2 = 1.60$ for SOQPSK-TG.

In case of PCM/FM, with symbol sequences given by

$$\boldsymbol{\alpha}_{\text{Tx}} = [1 \quad -1 \ 1 \ 1]$$

$$\boldsymbol{\alpha}_{\text{Rx}} = [1 \quad 1 \ -1 \ 1]$$

we obtain a minimum distance of $d_0^2 = 2.60$.

Appendix V - Laurent's Approximation

A detailed proof can be found in [12, 18]. We have

$$s(t; \boldsymbol{\alpha}) = \sum_n \sum_{k=0}^1 b_k[n] c_k(t - nT) \quad (7.20)$$

and

$$\tilde{s}(t; \boldsymbol{\alpha}) \simeq \sum_n b[n] p(t - nT). \quad (7.21)$$

We can find the normalized Mean Squared Error (MSE) using

$$\tilde{\sigma}^2 \triangleq \frac{\int_0^T E\{|\tilde{s}(t; \boldsymbol{\alpha}) - s(t; \boldsymbol{\alpha})|^2\} dt}{\int_0^T E\{s(t; \boldsymbol{\alpha})\} dt} \quad (7.22)$$

$$= \frac{1}{T} \int_0^T E\{|\tilde{s}(t; \boldsymbol{\alpha}) - s(t; \boldsymbol{\alpha})|^2\} dt. \quad (7.23)$$

We have to minimize the above equation by minimizing the integrand

$$\sigma^2 = E\{|\tilde{s}(t; \boldsymbol{\alpha}) - s(t; \boldsymbol{\alpha})|^2\} dt. \quad (7.24)$$

We then set the derivatives of $p(t)$ equal to zero to obtain the desired Laurent's approximation.

References

- [1] D. I. S. Agency. Department of Defense interface standard, interoperability standard for single-access 5-kHz and 25-kHz UHF satellite communications channels. Tech. Rep. MIL-STD-188-181B, Department of Defense, March 1999.
- [2] J. B. Anderson, T. Aulin, and C.-E. Sundberg. *Digital Phase Modulation*. Plenum Press, New York, 1986.
- [3] T. Aulin, C.-E. Sundberg, and A. Svensson. Viterbi detectors with reduced complexity for partial response continuous phase modulation. In *Proceedings of the National Telecommunications Conference, NTC'81*, pages A7.6.1–A7.6.7, New Orleans, LA, November/December 1981.
- [4] A. N. D'Andrea, A. Ginesi, and U. Mengali. Frequency detectors for CPM signals. *IEEE Transactions on Communications*, 43:1828–1837, Feb./Mar./Apr. 1995.
- [5] M. Geoghegan. Optimal linear detection of SOQPSK. In *Proceedings of the International Telemetry Conference*, October 2002.
- [6] W. H. Gerstaecker, F. Obernosterer, R. Mayer, and J. B. Huber. On pre-filter computation for reduced-state equalization. *IEEE Transactions on Communications*, 1:793–800, October 2002.
- [7] T. Hill. A non-proprietary, constant envelope, variant of shaped offset QPSK (SO-QPSK) for improved spectral containment and detection efficiency. In *Proceedings of IEEE MILCOM*, October 2000.

- [8] X. Huang and Y. Li. The PAM decomposition of CPM signals with integer modulation index. *IEEE Trans. Commun.*, 51(4):543–546, Apr. 2003.
- [9] N. Ibrahim, L. Lampe, and R. Schober. Bluetooth Receiver Design Based on Laurent’s Decomposition. *IEEE Transactions on Vehicular Technology*, 56:1856–1862, July 2007.
- [10] G. K. Kaleh. Simple coherent receivers for partial response continuous phase modulation. *IEEE J. Sel. Areas Comm.*, 7:1427–1436, Dec. 1989.
- [11] G. K. Kaleh. Differential detection via the Viterbi algorithm for offset modulation and MSK-type signals. *IEEE Transactions on Vehicular Technology*, 41:401–406, November 1992.
- [12] P. A. Laurent. Exact and approximate construction of digital phase modulations by superposition of amplitude modulated pulses (AMP). *IEEE Trans. Commun.*, 34:150–160, February 1986.
- [13] U. Mengali and M. Morelli. Decomposition of M -ary CPM signals into PAM waveforms. *IEEE Transactions on Information Theory*, 41:1265–1275, Sept. 1995.
- [14] E. Perrins. *Reduced Complexity Detection Methods for Continuous Phase Modulation*. Ph.D. dissertation, Brigham Young University, Provo, Utah, August 2005.
- [15] E. Perrins. Everything you wanted to know about double differential encoders but were afraid to ask. In *Proceedings of the International Telemetry Conference*, October 2006.
- [16] E. Perrins and M. Rice. PAM representation of ternary CPM. to be published in *IEEE Trans. Commun.*
- [17] E. Perrins and M. Rice. Optimal and reduced complexity receivers for M -ary multi-h CPM. In *Proceedings of the IEEE Wireless Communications and Networking Conference, WCNC’04*, pages 1165–1170, Atlanta, Georgia, March 2004.
- [18] E. Perrins and M. Rice. PAM decomposition of M -ary multi-h CPM. *IEEE Transactions on Communications*, 53(12):2065–2075, December 2005.

- [19] E. Perrins and M. Rice. Reduced-complexity approach to iterative detection of SOQPSK. *IEEE Trans. Commun.*, 55(7):1354–1362, Jul. 2007.
- [20] J. Proakis. *Digital Communications*. McGraw-Hill, New York, 2001.
- [21] R. Raheli, A. Polydoros, and C. K. Tzou. Per-survivor processing: A general approach to mlse in uncertain environments. *IEEE Transactions on Communications*, 43:354–364, Feb/Apr 1995.
- [22] Range Commanders Council Telemetry Group, Range Commanders Council, White Sands Missile Range, New Mexico. *IRIG Standard 106-00: Telemetry Standards*, 2000. (Available on-line at <http://www.ntia.doc.gov/osmhome/106.pdf>).
- [23] M. Simon. *Bandwidth-Efficient Digital Modulation With Application to Deep-Space Communication*. Wiley, New York, 2003.
- [24] M. K. Simon. Multiple-bit differential detection of offset QPSK. *IEEE Transactions on Communications*, 51:1004–1011, June 2003.
- [25] A. Svensson, C.-E. Sundberg, and T. Aulin. A class of reduced-complexity Viterbi detectors for partial response continuous phase modulation. *IEEE Transactions on Communications*, 32:1079–1087, Oct. 1984.